Environmental Modelling and Software 137 (2021) 104961

Contents lists available at ScienceDirect

Environmental Modelling and Software

journal homepage: http://www.elsevier.com/locate/envsoft

A framework for testing large-scale distributed soil erosion and sediment delivery models: Dealing with uncertainty in models and the observational data

Pedro V.G. Batista [a,*], J. Patrick Laceby [b], Jessica Davies [c], Teotônio S. Carvalho [d], Diego Tassinari [d], Marx L.N. Silva [d], Nilton Curi [d], John N. Quinton [e]

[a] Department of Environmental Geosciences, University of Basel, Basel, Switzerland
[b] Alberta Environment and Parks, Calgary, Canada
[c] Pentland Centre for Sustainability in Business, Lancaster Environment Centre, Lancaster University, Lancaster, UK
[d] Soil Science Department, Lavras Federal University, Lavras, Brazil
[e] Lancaster Environment Centre, Lancaster University, Lancaster, UK

ARTICLE INFO

Keywords:
Soil erosion models
Sediment loads
Sediment fingerprinting
RUSLE
SEDD
GLUE

ABSTRACT

Evaluating distributed soil erosion models is challenging because of the uncertainty in models and measurements of system responses. Here, we present an approach to evaluate soil erosion and sediment delivery models, which incorporates sediment source fingerprinting and sediment-rating curve uncertainty into model testing. We applied the Generalized Likelihood Uncertainty Estimation (GLUE) methodology to the Sediment Delivery Distributed model (SEDD) for a large catchment in Southeast Brazil. The model was not rejected, as 23.4% of model realizations were considered behavioral. Fingerprinting results and SEDD simulations showed a partial agreement regarding the identification of the main sediment sources in the catchment. However, grid-based estimates of soil erosion and sediment delivery rates were highly uncertain, which restricted the model's usefulness for quantifying sediment dynamics. Although our results are case-specific, similar levels of error might be expected in erosion models elsewhere. The representation of such errors should be standard practice.

1. Introduction

Spatially-distributed soil erosion and sediment delivery models have received significant attention from the erosion modelling community, arguably due to their potential usefulness for identifying erosion-prone areas and the main sediment sources within large catchments. However, evaluating the usefulness of such models is inherently challenging: measurements of model parameters and system responses are necessarily uncertain, the spatial and temporal resolution of models and observational data are frequently divergent, and the definition of what is a useful model is often subjective (Oreskes and Belitz, 2001). Moreover, our ability to measure erosion rates across landscapes is limited and methods for doing so are known to be flawed (Parsons, 2019). Since model evaluation is an essential step to recognize model failure and to consequently gain knowledge about the modeled phenomena; how should we proceed in face of the aforementioned challenges?

Currently, the most common approach for testing distributed erosion models at the catchment scale is based on a comparison between observed and modeled outlet sediment loads. The estimation of observed loads usually rely on I) suspended solid measurements and/or sediment rating curves (Didoné et al., 2015; Jain and Ramsankaran, 2018; Krasa et al., 2019; Vigiak et al., 2015); II) temporally-spaced bathymetric surveys or excavations of ponds and reservoirs (de Vente et al., 2008; Eekhout et al., 2018; Tanyaş et al., 2015); or III) radiometric dating of lake sediment cores (Smith et al., 2018b). Although a comparison against sediment loads can give an indication of a models capability to simulate sediment transport rates at the outlet of a catchment, it provides no information on the adequacy with which models simulate erosion patterns or identify sediment sources. Moreover, models have been known to reproduce observed outlet sediment loads for the wrong reasons, through misrepresenting internal catchment processes (see Pontes, 2017 for an example).

Therefore, the outlet-based approach for testing distributed erosion models has received criticism (Favis-Mortlock et al., 2001; Govers,

* Corresponding author.
E-mail address: pedro.batista@unibas.ch (P.V.G. Batista).

https://doi.org/10.1016/j.envsoft.2021.104961
Accepted 4 January 2021
Available online 8 January 2021
1364-8152/

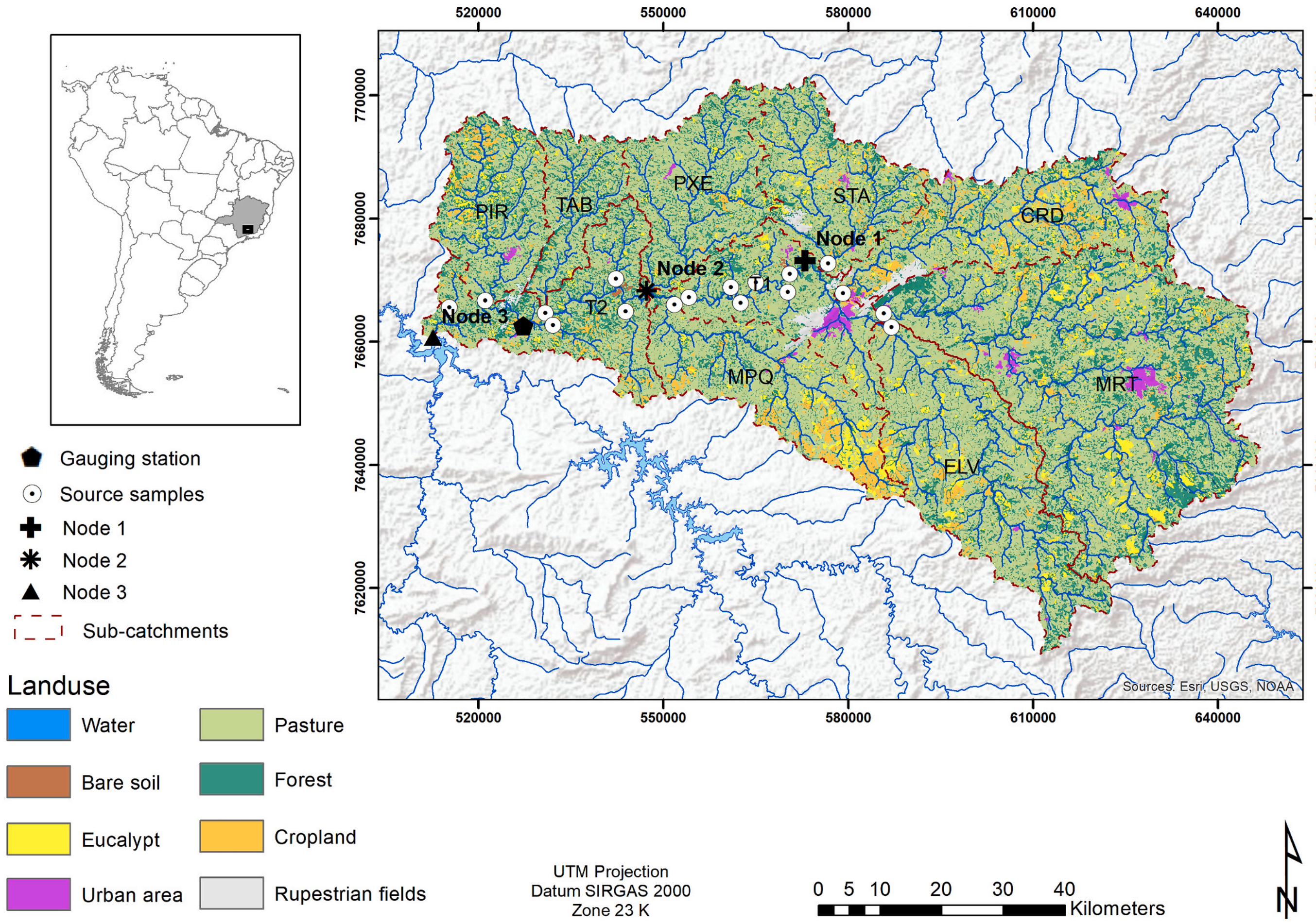

Fig. 1. Location of the Mortes River basin and the land use map of the catchment. Sub-catchments and sampling locations for sediment fingerprinting are also displayed. Legend: MRB: Mortes River basin; CRD: Carandaí River sub-catchment; ELV: Elvas River sub-catchment, MPQ: Mortes Pequeno River sub-catchment; MRT: Mortes River sub-catchment; PIR: Pirapetinga River sub-catchment; PXE: Peixe River sub-catchment; STA: Santo Antônio River sub-catchment; T1: mid catchment area; T2: lower catchment area; TAB: Tabões River sub-catchment.

2011; Jetten et al., 2003; Parsons et al., 2009), and modelers have pursued other sources of data to evaluate internal process representations. For instance, field monitoring of erosion features combined with volumetric measurements of rills, gullies, and sediment deposition drapes can provide spatially referenced information of internal erosion dynamics that are commensurate with model simulations (Evans and Brazier, 2005; Takken et al., 1999; Van Oost et al., 2005). Alternatively, tracing techniques have been used to estimate medium to long-term soil redistribution rates, which are also comparable to distributed erosion model outputs (Lacoste et al., 2014; Porto and Walling, 2015; Walling et al., 2003; Warren et al., 2005). More recently, Zweifel et al. (2019) and Fischer et al. (2018) demonstrated how aerial images could be used to visually classify the severity of erosion features, and how this classification was appropriate to assess the capability of spatially distributed models to relatively rank erosion-prone areas.

While the previously described sources of data for model testing are useful for evaluating simulations of on-site erosion, they offer little information about sediment transport to water courses and subsequent off-site erosion impacts. Therefore, they cannot be used to test the sediment delivery or routing components of distributed erosion models. Models such as WaTEM/SEDEM (Van Oost et al., 2000; Van Rompaey et al., 2001; Verstraeten et al., 2010), Morgan-Morgan-Finey (MMF) (Morgan, 2001; Morgan et al., 1984), and the Sediment Delivery Distributed model (SEDD) (Ferro and Minacapilli, 1995; Ferro and Porto, 2000) represent hillslope connectivity to the stream network either by routing sediment transport capacity along the flowpath or by estimating a topography-based sediment delivery ratio. These models are therefore not only able to simulate how much sediment is delivered to water courses, but also to identify where it comes from. To evaluate the quality of such simulations, quantitative data of sediment provenance is necessary.

A technique that provides quantitative apportionments of sediment provenance is sediment source fingerprinting. In this approach, physical and biogeochemical attributes of sink sediments are used to trace their origin from potential upstream sources (Klages and Hsieh, 1975; Yu and Oldfield, 1989; Walling and Woodward, 1995). Relative source contributions are then calculated by solving end-member un-mixing models based on source and sink sediment tracer concentrations (Collins et al., 1997; Cooper et al., 2014; Laceby and Olley, 2015). Such estimates are conceivably comparable to the outputs of distributed soil erosion models with a sediment routing/delivery component. However, a meaningful comparison requires fingerprinting source stratifications to be reasonably analogous to model outputs.

An interesting example was presented by Wilkinson et al. (2013), in which sediment fingerprinting was used to model the contributions of different erosion processes (i.e. surface and subsurface) to sediment loads in the Burdekin River basin, Australia (130,000 km^2). The resulting source apportionments were compared to the Sediment budget river Network (SedNet) model outputs (Wilkinson et al., 2009). Since SedNet calculates sediment budgets by differentiating inputs from different erosion processes (i.e. gullies, sheetwash), results provided a useful analogy. Likewise, Borrelli et al. (2018) were able to compare

Table 1
Physiographic attributes of the Mortes River basin and its sub-catchments.

	MRB	CRD	ELV	MPQ	MRT	PIR	PXE	STA	T1	T2	TAB
Soil class	Area (%)										
Dystrustepts	35.2	24.3	30.2	37.6	49.5	0.0	36.7	38.6	94.8	6.5	0.0
Acrudoxes	0.7	0.0	0.0	0.3	0.0	1.0	0.0	0.0	0.0	3.3	10.0
Hapludoxes	48.2	74.0	61.0	55.8	18.9	89.0	47.4	60.5	1.0	70.9	60.0
Rhodudults	4.6	0.0	0.0	0.0	0.0	10.0	15.1	0.0	0.5	18.3	30.0
Paleudults	10.2	0.0	8.8	5.7	30.9	0.0	0.0	0.0	0.0	0.0	0.0
Ustorthents	0.5	1.7	0.0	0.0	0.7	0.0	0.7	0.8	0.0	0.0	0.0
Rocky outcrops	0.6	0.0	0.0	0.5	0.0	0.0	0.0	0.0	3.8	1.0	0.0
Land use	Area (%)										
Bare soil	0.1	0.0	0.1	0.0	0.0	0.2	0.0	0.0	0.6	0.4	0.0
Cropland	4.6	11.6	3.9	11.1	2.7	5.0	1.4	3.6	0.7	4.8	1.3
Eucalypt	5.2	5.8	5.9	8.5	5.8	6.2	3.0	5.1	2.3	2.5	2.3
Forest	21.6	18.0	18.6	14.2	25.1	25.5	22.1	20.4	22.8	27.5	24.4
Pasture	66.2	60.0	71.2	65.3	64.3	61.9	73.1	68.5	70.5	62.6	71.3
Rupestrian fields[a]	1.0	2.7	0.0	0.5	0.2	0.6	0.0	2.0	1.6	1.1	0.5
Urban area	1.1	1.8	0.1	0.3	1.8	0.7	0.3	0.4	0.5	0.1	0.0
Water	0.2	0.2	0.1	0.1	0.1	0.0	0.0	0.0	1.0	0.8	0.1
Slope	(θ)										
Mean	9.1	8.3	8.9	7.8	9.9	8.4	9.1	9.9	9.7	8.3	9.7
Std. Dev.	5.2	4.8	5.0	4.4	5.7	4.5	5.0	5.3	5.5	4.9	5.4
Elevation	(m)										
Min.	807	890	892	869	892	826	865	890	865	807	864
Max.	1414	1407	1412	1191	1414	1209	1339	1312	1246	1239	1205
Mean	1035	1073	1061	996	1091	971	1035	1035	956	931	988
Area	(km^2)										
	6608	676	875	566	1817	424	510	509	446	526	259

Legend: MRB: Mortes River basin; CRD: Carandái River sub-catchment; ELV: Elvas River sub-catchment, MPQ: Mortes Pequeno River sub-catchment; MRT: Mortes River sub-catchment; PIR: Pirapetinga River sub-catchment; PXE: Peixe River sub-catchment; STA: Santo Antônio River sub-catchment; T1: mid catchment area; T2: lower catchment area; TAB: Tabões River sub-catchment.

[a] Grassland herbaceous/sub-shrubby formation that is commonly found on quartzitic ridges and other rocky outcrops.

land use source apportionments from Alewell et al. (2016) to WaTEM/SEDEM model outputs in a 41 km^2 catchment on the Swiss Plateau.

However, a difficulty when testing erosion models in particular and environmental models in general arises from the epistemic uncertainties in model structures, parameter estimation, and the forcing/testing data (Beven, 2019). That is, uncertainty is a result of a lack of knowledge about I) the modeled phenomena: models are inherently flawed approximations of reality; II) the model parameters: we cannot measure model parameters in every point in space and even if we could, parameters are often empirical abstract aggregations that require calibration; and III) the observational data: erosion is a highly variable phenomenon and our methods for measuring it are somewhat inadequate. Testing models as hypotheses therefore requires representing the uncertainties in both models and the things we call observational data of systems responses (Beven, 2018). It also requires a clear definition of model purpose and of the limits of acceptability of model error (Beven, 2006, 2009). These concepts provide the foundation of the Generalized Likelihood Uncertainty Estimation (GLUE) (Beven and Binley, 1992) methodology, in which Monte Carlo simulations are used to create a large number of possible model realizations by sampling uncertain model parameters. If the response surface does not produce acceptable realizations of the observational data, then the model itself can be rejected as not useful for prediction – at least under the testing conditions (Beven, 2009).

Although sediment fingerprinting models are now consistently applied in stochastic structures, usually relying on Monte Carlo simulations (Evrard et al., 2013; Pulley et al., 2016; Smith and Blake, 2014) or Bayesian modelling (Blake et al., 2018; Cooper and Krueger, 2017), soil erosion models are more frequently used in a deterministic fashion. Moreover, outlet sediment loads, which are the common forcing/testing data with which models are evaluated, are also represented deterministically. Therefore, an uncertainty-based framework for incorporating sediment fingerprinting into soil erosion model testing is lacking.

In this study we present a novel approach to evaluate spatially distributed soil erosion/sediment delivery models that represents the uncertainties in both models and observational data. Since we understand that the purpose of spatially distributed models is to not only to provide acceptable simulations of outlet transport rates, but also to represent sediment dynamics within a catchment, we use sediment loads and sediment fingerprinting source apportionments as model evaluation data. By use of the GLUE methodology, we apply the SEDD model to a ~6600 km^2 river basin in southeast Brazil. Although GLUE has been used in other soil erosion modelling applications, our testing framework is the first to define limits of acceptability of model error according to the uncertainty in the observational sediment load data. A further novelty is the evaluation of behavioral model simulations against sediment fingerprinting source apportionments, which have been stratified based on a hierarchical tributary design that facilitates model comparisons along different stages of sediment transport. Our approach is implemented on free GIS software and programming languages, being fully reproducible and/or adaptable elsewhere. The outcomes of this research therefore provide a much-needed open source framework for incorporating uncertainty analysis into distributed soil erosion models applications. Moreover, it demonstrates how sediment fingerprinting, and potentially other sources of data, can be assimilated into model testing within a stochastic structure.

2. Methods

2.1. Catchment description

The Mortes River drains an area of approximately 6600 km^2 in the south of the State of Minas Gerais, Brazil (Fig. 1). The river's headwaters are in Mantiqueira Mountain Range and it flows until its confluence with the Grande River, at the Funil hydroelectric power plant reservoir. Elevation within the basin ranges from 1414 m to 807 m. According to Köppen's classification, the climate in the area is predominantly 'humid subtropical with dry winters and warm summers' (i.e. a Cwb climate type) (Alvares et al., 2013). Average annual rainfall is approximately 1500 mm (Fick, 2017), which is almost entirely concentrated in the spring and summer months.

Hapludoxes (48%) and Dystrustepts (35%) are the main soil classes in the basin (Table 1). The first are very deep, highly weathered-leached soils, while the latter are much less pedogenetically developed, shallow, and erosion-prone. Most of the catchment is occupied by pastures (66%), often degraded by over-grazing and/or lack of adequate management. Remaining forest areas (22%) are mostly found on ridges and buffer strips along the stream network. Croplands, which are mostly composed of maize fields for silage production, occupy a small portion of the catchment area (5%). Eucalypt forests (5%) are commonly planted for charcoal manufacturing. Most of the agricultural areas, notably in the Carandaí, Mortes Pequeno, and Pirapetinga sub-catchments, are associated with the occurrence of Hapludoxes (Fig. 1, Table 1). Dystrustepts support extensive pastures for raising dairy cattle and/or eucalypt plantations.

The Mortes River basin was chosen for this study due to the availability of continuous sediment concentration and discharge data from the Ibituruna gauging station (Fig. 1). Although water discharge records are frequently made available by the Brazilian Water Agency, sediment concentration data are difficult to obtain. Moreover, field observations and bathymetric surveys have shown that the Mortes River delta is the main sedimentation zone in the Funil reservoir. Although the reservoir was built in 2003, the high sedimentation rates in Mortes River already impede navigation near its delta.

2.2. Sediment load data

Suspended sediment concentration (mg L^{-1}) and water discharge ($m^3\ s^{-1}$) were monitored in the Ibituruna gauging station (Fig. 1) from March 2008 to December 2012 (Batista et al., 2017). Measurements were taken on an approximately monthly basis, resulting in 44 observations. In order to estimate long-term sediment loads, we fitted a sediment rating curve relating suspended solid concentration to water discharge by ordinary least squares. Both variables were log-transformed, as the relationship between sediment concentration and discharge in the log-scale is approximately linear (Vigiak and Bende-michl, 2013). The goodness-of-fit of the linear model was visually assessed with residual and Quantile-Quantile plots. These and all other statistical analyses here presented were performed with the R programming language (R Core Team, 2019).

In order to propagate the error of the fitted model, 10^4 posterior simulations of the model coefficients were generated by an informal Bayesian function from the R package *arm* (Gelman and Hill, 2007). This function uses the model residual standard errors to create multivariate normal distributions of model coefficients, thus preserving their correlation when estimating posterior simulations. Next, daily sediment concentrations values were calculated based on continuous (mean daily) discharge records from the Brazilian Water Agency for the Ibituruna gauging station (1992–2013) and the simulations of model coefficients. These concentration values were used to estimate daily sediment loads (ton day^{-1}), which were subsequently aggregated into monthly, annual, and average annual transport rates. In summary, the 10^4 simulations of daily sediment concentrations were used to propagate the rating curve uncertainty when calculating long-term sediment loads. As pointed out by Vigiak and Bende-michl (2013), this approach only quantifies the regression uncertainty, and the actual errors associated to sediment load calculations might be underestimated. More detailed descriptions of Bayesian and bootstrapping methods for propagating the uncertainty of sediment rating curves can be found in Rustomji and Wilkinson (2008) and in Vigiak and Bende-michl (2013).

2.3. Sediment fingerprinting data

2.3.1. Sampling design and sample collection

In order to facilitate a comparison between SEDD model outputs and fingerprinting source apportionments, we developed a tributary sampling design, in which sub-catchments of the Mortes River basin were treated as end-member sediment sources. In addition, we adopted a hierarchical approach for sink sediment sampling (Blake et al., 2018; Boudreault et al., 2019; Koiter et al., 2013). That is, considering the disconnectivity of the sediment cascade on large river basins due to the variability of residence times of sediment storage (Koiter et al., 2013), we understood it was important to sample sink sediments at different nodes of the main river channel (Fig. 1). As a result of our sampling design, three nodes with four potential upstream sources each were stratified within the catchment.

Node 1 has four main tributaries: the Mortes River (MRT) itself before its confluence with the Elvas River (ELV), the Carandaí River (CRD), and the Santo Antônio River (STA). Due to our hierarchical approach, Node 1 sediments become a potential source of the next downstream node. Hence, Node 2 sources are comprised by the Mortes Pequeno River (MPQ), the Peixe River (PXE), the set of small tributaries in the mid catchment (T1), and Node 1. Similarly, Node 3 on the catchment outlet receives sediments from the Pirapetinga River (PIR), the Tabões River (TAB), the set of small tributaries in the lower catchment (T2), and Node 2.

Sediment sampling was conducted in two different periods to represent transport dynamics during the well-defined seasons of the local climate. During September 2017 (dry season), all nodes and sources were sampled. In February 2018, during the rainy season, we retrieved extra samples from the sink sediment nodes.

Source samples were taken from lag-deposits of tributaries near their confluence with the main river channel. The uppermost layer (1–2 cm) of freshly deposited sediments from river margins was scrapped with a plastic trowel, and approximately 15 scrapes were combined into one individual sample. We collected a total of 20 composite samples per each tributary, except for sources T1 and T2. These sources are comprised by a set of small tributaries that drain directly to the Mortes River (Fig. 1). Hence, 25 and 17 samples were retrieved in T1 and T2, respectively (4–5 samples from each small tributary).

Sampling sink sediments from Nodes 1 and 2 followed the same methods described above. During the dry season 20 samples were collected from each of these nodes, whereas during the rainy season, 12 and 20 samples were retrieved from Nodes 1 and 2, respectively. Given that the Mortes River flows into the Funil reservoir, samples from Node 3 were taken from the bottom of the shallow river delta, before its confluence with the Grande River. At the node 3 site, 26 and 12 composite samples were collected during the dry and rainy seasons, respectively.

2.3.2. Laboratory analyses

Sediment samples were oven-dried at 60 °C and dry-sieved with a 0.2 mm mesh. Subsequently, total concentration of the 21 following elements was determined by inductive coupled plasma optical emission spectrometry (ICP OES): Al, As, Ba, Ca, Cd, Ce, Co, Cr, Cu, Fe, K, La, Mg, Mn, Ni, Pb, Se, Ti, V, Zn, Zr. The <0.2 mm particle size was selected according to the texture analysis of the sink sediments from Node 3, at the Mortes River delta (Supplementary Material Table 1). The analysis indicated that an important fraction of the target sediments were composed of fine sand (0.2–0.05 mm), and that fractionating samples to a finer size could lead to unrepresentative results.

2.3.3. Element selection

The first step of tracer selection is to investigate the composition of source and sink sediments. Here, we started with an exploratory analysis by visually examining box-plots of element concentrations. Next, a range test was performed to verify if sink element concentrations were well bounded by the source mixing polygon. That is, if element contents on sink sediments are enriched or depleted in relation to source samples, then there is evidence that elements might not be behaving conservatively during sediment transport or there is a missing source (Laceby et al., 2017; Smith and Blake, 2014). Moreover, a mismatch of element concentrations on source and sink sediments may compromise the numerical solutions of the un-mixing models (Collins et al., 2013). The range test therefore aims not only to eliminate elements plotting outside the mixing polygon from further analyses, but also to provide an initial insight into the quality of the geochemical data.

Different approaches have been employed for analyzing conservative behavior and for performing range tests (Smith et al., 2018a; Wilkinson et al., 2015). Although earlier research might have focused on maximum and minimum tracer values, distribution-based un-mixing models (Bayesian or frequentitst) requires an examination of the distributions of tracer concentrations. Considering the structure of the bootstrapping approach we employed for solving our un-mixing model, we adopted a mean and standard deviation range test. That is, we assumed that means and standard deviations of log-transformed tracer concentrations on sink sediments should plot within the means and standard deviations of the source log-transformed tracer concentrations. This ensures that, during the Monte Carlo simulation, sampled sink element contents will always be within the source range. The means and standard deviation range test was performed locally for each node and sampling season.

Given the heterogeneity of land uses and geological/pedological backgrounds of the sub-catchments comprising sediment sources in the Mortes River basin (i.e. catchments do not display a definite pattern of source signal development agents – Table 1), a process-based approach to element selection (e.g. Batista et al., 2019; Koiter et al., 2013; Laceby et al., 2015) was not appropriate to this research. Hence, we adopted a more common statistical procedure, in which elements passing the range test were submitted to a step-wise forward Linear Discriminant Analysis (LDA) (niveau = 0.1). This approach aims to define a minimum set of tracers that maximize source discrimination, and elements selected by the LDA were used for modelling. Again, the procedure was repeated for all nodes and sampling seasons.

2.3.4. Un-mixing modelling

Relative sediment source contributions were calculated by minimizing the sum of squared residuals (SRR) of the un-mixing model:

$$SSR = \sum_{i=1}^{n} [(C_i - \sum_{s=1}^{m} P_s S_{si}) \Big/ C_i]^2 \tag{1}$$

where: n is the number of elements used for modeling, C_i is the concentration of element i in the target sediment, m is the number of sources, P_s is the optimized relative contribution of source s, and S_{si} is the concentration of element i in source s. Optimization constraints were set to ensure that source contributions P_s were non-negative and that their sum equaled 1.

In order to quantify the uncertainty in the un-mixing model source apportionments, we employed the bootstrapping methods described in Batista et al. (2019). The model was solved by a Monte Carlo simulation with 2500 iterations. For each iteration, log-transformed element concentrations were sampled from multivariate-normal distributions generated from the source and sink geochemical data. During the Monte Carlo simulation, values were back-transformed by an exponential function. Log-transformation was applied to avoid sampling negative element concentrations and to force a near-normal distribution on the typically skewed sediment geochemistry data. The optimization function was scripted with the R package *Rsolnp* (Ghalanos and Theussl, 2015), whereas the Monte Carlo simulation (here and elsewhere in this study) with the package *foreach* (Calway et al., 2017).

2.4. SEDD model description

The SEDD model calculates a spatially distributed sediment delivery ratio *SDRi* that expresses the proportion of eroded sediments that are delivered to the stream network (Ferro and Minacapilli, 1995; Ferro and Porto, 2000). The model does not represent channel erosion or deposition processes, and sediments reaching the stream network are assumed to reach the catchment outlet. Following a grid based structure, the *SDRi* was calculated as:

$$SDR_i = \exp(-\beta \frac{l_i}{s_i}) \tag{2}$$

where: SDR_i is the soil delivery ratio of a grid cell I, β is a catchment specific empirical parameter (m^{-1}), l_i is the flow length from cell i to the nearest stream channel (m) along the flow path, and s_i is the slope of cell i ($m\ m^{-1}$).

Typically, the empirical parameter β is calibrated to minimize the errors of sediment load predictions (Fernandez et al., 2003; Fu et al., 2006; Lin et al., 2016), whereas the flow length and slope parameters can be derived from DEM processing.

The *SDRi* grid is used to calculate area specific sediment yields (*SSYi*) (ton $ha^{-1}\ yr^{-1}$), which quantifies the amount of sediments that are delivered from cell i to the stream network:

$$SSY_i = SDR_i A_i \tag{3}$$

where: SSY_i is the specific sediment yield for a grid cell I, SDR_i is the soil delivery ratio for a grid cell i, and A_i is the annual soil loss computed by Revised Universal Soil Loss Equation (RUSLE) for a grid cell i.

RUSLE estimates average annual erosion rates by the following empirical equation (Renard et al., 1997):

$$A = R*K*LS*C*P \tag{4}$$

where: A is soil loss per unit area (t $ha^{-1}\ yr^{-1}$); R is the rainfall and runoff erosivity factor (MJ mm $ha^{-1}\ h^{-1}\ yr^{-1}$), K is soil erodibility factor (t ha h $ha^{-1}\ MJ^{-1}\ mm^{-1}$), LS is the topographic factor, representing slope length and steepness (dimensionless), C is the cover management factor (dimensionless), and P is the support practice factor (dimensionless).

As the SEDD model neglects channel deposition, the total sediment yield at the catchment outlet can be calculated as the sum of *SSYi* values (weighted by cell area). Equivalently, the mean of *SSYi* values corresponds to the area specific sediment yield in the catchment, and the same calculations can be employed at sub-catchment scale. With this approach, sub-catchment relative contributions can be estimated based on SEDD results.

Of note, we chose SEDD for three main reasons: I) the model requires calibration, which makes it particularly suitable for GLUE; II) the model has few parameters, which facilitates computer processing when making a large number of simulations with large spatial datasets; and III) the model is RUSLE-based, which gives us the opportunity to scrutinize the uncertainty associated to the most widely-used soil erosion model in world.

2.5. GLUE

The GLUE methodology can be summarized in five decision steps (Beven, 2009), which include i) the definition of a likelihood measure to evaluate model realizations; ii) definition of a rejection criteria for non-behavioral model realizations; iii) definition of uncertain model parameters; iv) definition of distributions to characterize parameter uncertainty; and v) definition of a simulation method for creating model realizations.

We did not establish a formal likelihood measure to evaluate model realizations, as the rejection criteria for non-behavioral simulations was set according to an actual range of system responses. That is, all model

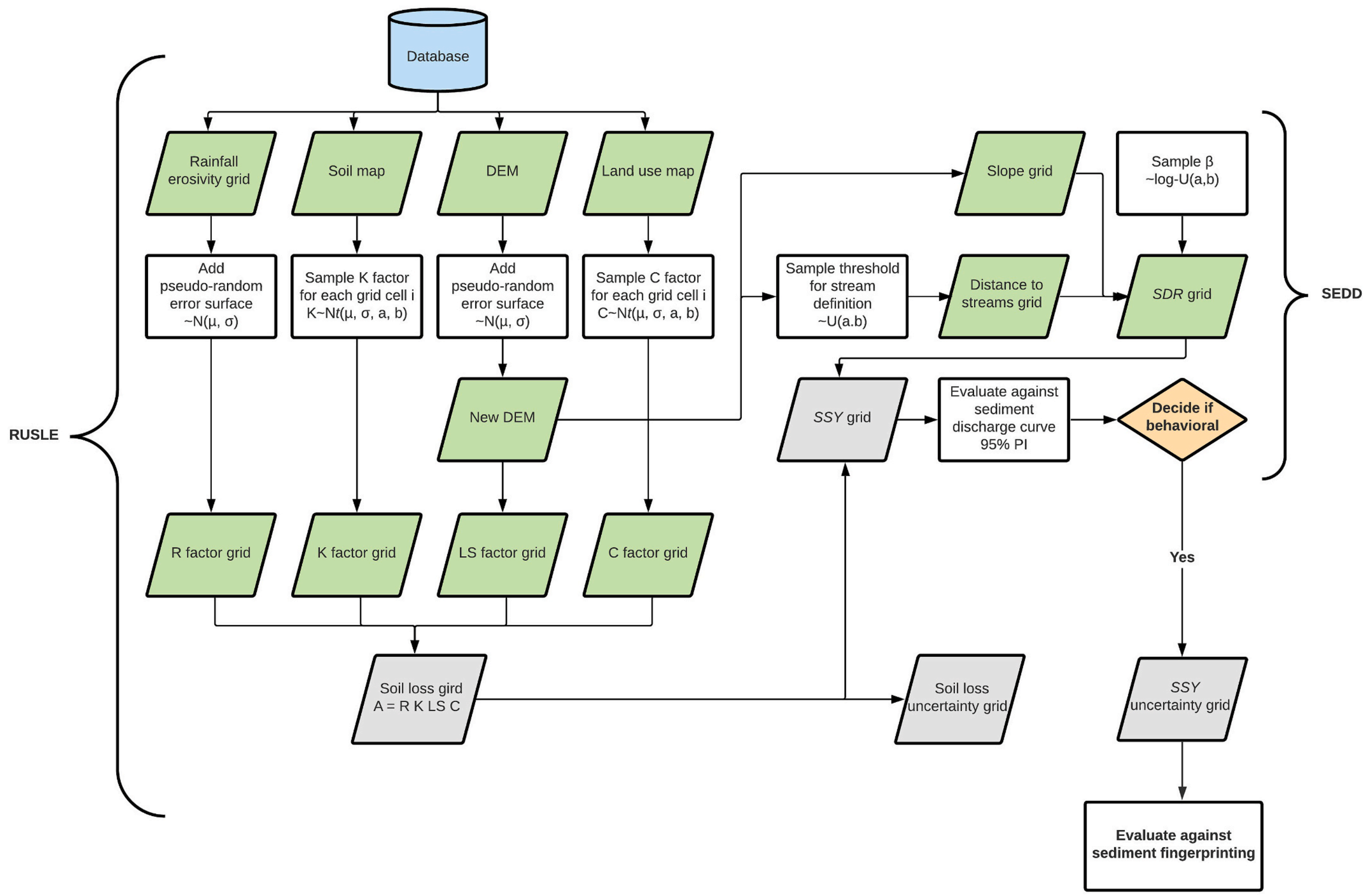

Fig. 2. Flowchart of the Monte Carlo simulation used for generating RUSLE and SEDD model realizations within the GLUE framework.

realizations which produced sediment load responses within the 95% prediction interval of the sediment load rating curve were considered behavioral. Since the SEDD temporal scale is inherited from the RUSLE, the model simulates long-term average annual sediment yields. Therefore, for comparison purposes the sediment rating curve estimates were aggregated into a 22 years average.

Model realizations were generated by a Monte Carlo simulation with 1000 iterations (Fig. 2). SEDD parameter β was sampled from a log-uniform distribution, with minimum and maximum parameters retrieved from typical values reported in the literature (min = 0.000001 m^{-1}, max = 0.1 m^{-1}) (e.g. Porto and Walling, 2015; Taguas et al., 2011). We used a log-uniform distribution to ensure that the extreme values of this broad range were sampled during the simulation. The threshold for stream definition, which affects drainage density and therefore distance to streams (l_i), was sampled from a uniform distribution (min = 50,000 m^2, max = 5,000,000 m^2). To represent the uncertainty in the DEM derived model variables, we created a pseudo-random error surface for each model iteration. Mean and standard deviation of DEM errors were retrieved from the NASA SRTM report (Rodriguez et al., 2006) ($\mu = 1.7$ m, $\sigma = 4.1$ m) and used to create a normally distributed error field, which was added to the original DEM. All terrain attributes used in the models were then calculated within the Monte Carlo simulation.

All herein described spatial analyses were supported by SAGA GIS (Conrad et al., 2015) and the R package *RSAGA* (Brenning and Bangs, 2015). The R scripts used for model implementation and uncertainty analysis are provided as Supplementary Material along with raw fingerprinting and discharge data. Additional R packages used in the simulations include: *raster* (Hijmans and Van Etten, 2012), *trucnorm* (Mersmann et al., 2018), *doParallel* (Ooi et al., 2019), *rgdal* (Bivand et al., 2019), *WGCNA* (Langfelder and Horvath, 2019).

Since we understood that RUSLE factors were not parameters requiring calibration or conditioning, but instead uncertain model variables, we performed a forward uncertainty analysis, similarly to Biesemans et al. (2000) and Van Rompaey and Govers (2002). Although this can be seen as a separate analysis, RUSLE error was propagated into SEDD simulations, as we explain in the following.

The forward error analysis was performed with a Monte Carlo simulation with 1000 iterations. In order to represent the uncertainty in the RUSLE R factor, we first calculated a deterministic rainfall erosivity map (Supplementary Material Fig. 1). This was carried out with average monthly and annual rainfall grids from WorldClim (Fick, 2017) and the regression equation developed by Aquino et al. (2014). This regression equation estimates annual (or average annual, in this case) EI_{30} index values, and it was originally fitted using detailed rainfall data from the Municipality of Lavras. For each iteration of the Monte Carlo simulation, we added a normally distributed error surface to the deterministic rainfall erosivity map, with mean equal zero and a standard deviation equal to 10% of mean deterministic R factor for the catchment.

For the K factor, we created truncated normal distributions for each

Table 2
Parameters of the truncated normal distribution of K factor values (t ha h ha^{-1} MJ^{-1} mm^{-1}) for each soil class in the Mortes River basin.

Soil class	Mean	Standard dev.	Minimum	Maximum
Dystrustepts	0.035	0.01	0.01	1
Acrudoxes	0.012	0.01	0.001	1
Hapludoxes	0.015	0.01	0.001	1
Rhodudults	0.017	0.01	0.005	1
Paleudults	0.02	0.01	0.005	1
Ustorthents	0.05	0.01	0.03	1
Rocky outcrops	0.00001	0.00001	0.00001	1

Table 3
Parameters of the truncated normal distribution of C factor values for each land use class in the Mortes River basin.

Land use	Mean	Standard dev.	Minimum	Maximum
Bare	0.8	0.2	0.6	1
Cropland	0.088	0.045	0.02	1
Eucalypt	0.015	0.03	0.0005	1
Forest	0.001	0.003	0.0001	1
Pasture	0.01	0.02	0.001	1
Rupestrian vegetation	0.001	0.005	0.0001	1

soil class occurring in the catchment soil map (FEAM, 2010). The discrete soil map was rasterized and, for each simulation, a grid cell erodibility value was sampled according to its corresponding soil class. Distribution parameters were set according to published K factor values for Brazilian soils (see Silva et al., 2019). Although in general there were not enough different estimations of K factor values for individual soil classes to create data-based probability distributions, we used the available published data and our own interpretation to infer distribution parameters (Table 2).

Uncertainty in the LS factor was represented following the DEM error propagation described above. Slope (rad) and catchment area (m^2) grids were created for each model iteration. These grids were subsequently used to calculate the LS factor with the equation of Desmet and Govers (1996). A maximum threshold of 10,800 m^2 was enforced to the catchment area grid, which corresponds to maximum flow length of 360 m for a 30 m resolution DEM. This was performed to avoid spuriously high LS factor values in flow concentration areas, as usually carried out in RUSLE applications (Panagos et al., 2015; Schmidt et al., 2019). The maximum threshold was empirically defined, based on remote sensing and field observations from the study area. In this case, lower flow accumulation thresholds would lead to hillslopes being identified as flow concentration zones (e.g. gullies, ravines, hollows), when rill and interril should still be more representative of the erosion processes.

Similarly to the K factor, errors in the C factor estimation were propagated by creating truncated normal distributions for individual land use classes (Table 3). The land use grid was produced using 30 m resolution Landsat 8 Surface Reflectance images from 2013 and the methods described in Batista et al. (2017). Since no widespread support management practices are found in the catchment agricultural areas, no specific procedure was applied to represent P factor uncertainty. However, the C factor distribution parameters for cropland and eucalypt were set to reflect occasional contour cropping and/or crop residue management. A summary of published C factor values for typical Brazilian land uses and crop management can be found in Silva et al. (2019).

The resulting RUSLE model realizations were used as input for the SEDD model simulations. Moreover, we performed a sensitivity analysis by fixing each model factor and sampling the remaining variables in new Monte Carlos simulations, each with 1000 iterations. This enabled us to evaluate the proportion of model variance explained by each factor.

It should be highlighted that forward error propagation is essentially

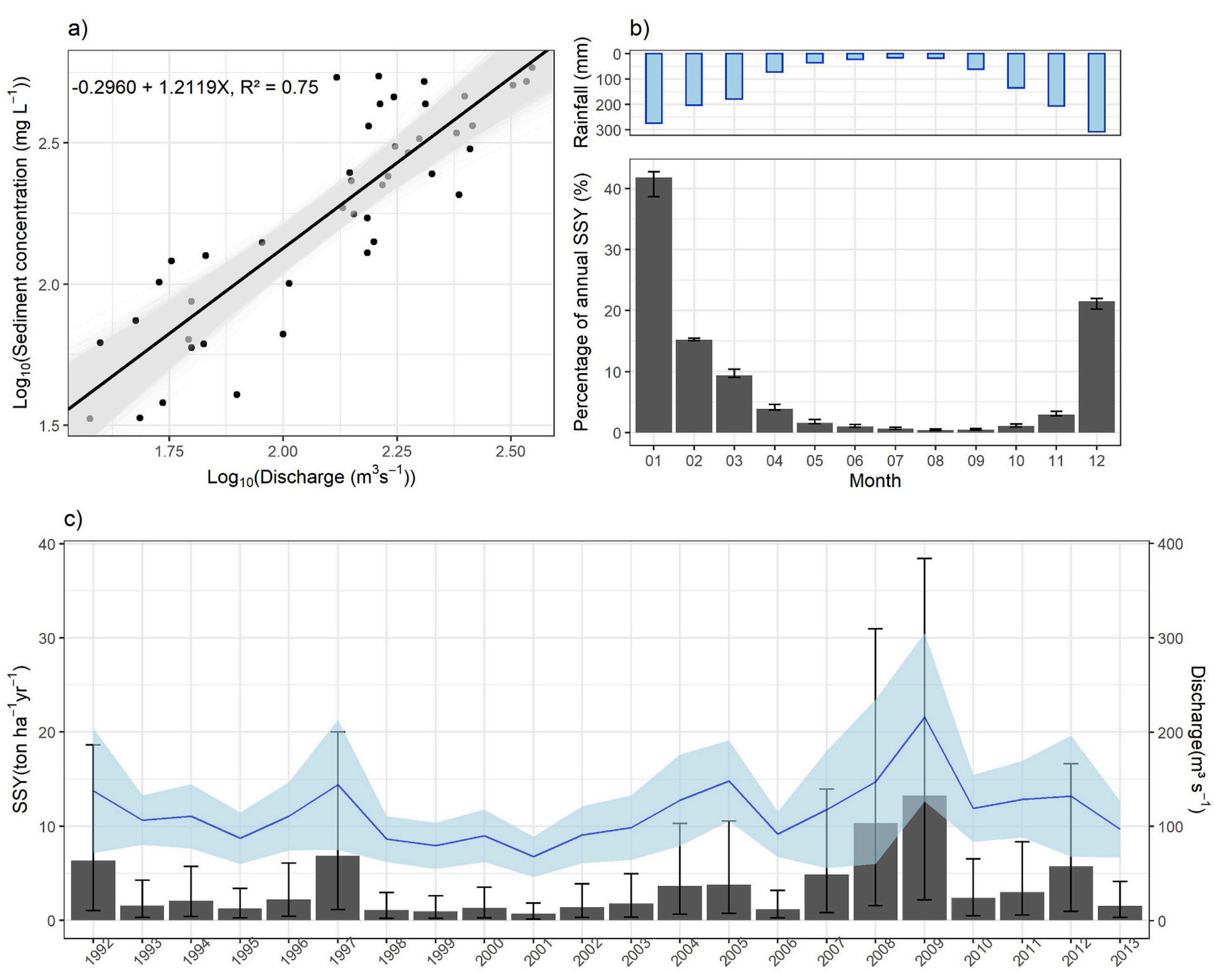

Fig. 3. a) Sediment rating curve: dark line represents a deterministic model fit and faded gray lines represent the 1000 simulations used to propagate the regression uncertainty, b) WorldClim monthly rainfall data for the Mortes catchment and percentage of annual SSY, c) annual SSY (bars) and discharge (line) for the Mortes River. Error bars represent 95% prediction intervals. Shaded area represents 95% confidence interval.

Table 4
Selected elements by the range test and the forward LDA for each node and season, along with the LDA reclassification accuracy.

Node	Season	Selection step	Selected elements	% of correctly classified samples
1	Dry	Range test	Al, As, Ba, Cd, Ce, Co, Cr, Fe, K, La, Mg, Mn, Pb, Se, Ti, V	
		LDA	Al, Ba, Cd, Ce, Co, Cr, Fe, K, Mg, Mn, Ti, V	100
	Rainy	Range test	Al, As, Ba, Ca, Ce, Co, Cr, Fe, K, Ka, Mg, Mn, Ni, Pb, Se, Ti, V, Zr	
		LDA	Al, Ba, Ca, Co, Cr, K, Mg, Ni, Se, V, Zr	100
2	Dry	Range test	Al, As, Ba, Ca, Cd, Ce, Co, Cr, Fe, K, La, Mg, Ni, Se, Ti, V, Zr	
		LDA	As, Ca, Ce, K, La, Mg, Ni, Se, Ti, Zr	100
	Rainy	Range test	Al, As, Ba, Ca, Cd, Ce, Co, Cr, Fe, K, La, Mn, Ni, Pb, Se, Ti, V, Zr	
		LDA	As, Ca, Ce, Co, K, La, Mn, Pb, Se, Ti, Zr	100
3	Dry	Range test	Ba, Ca, Cd, Ce, Cr, Fe, K, La, Ni	
		LDA	Ca, Cd, Ce, Cr, K, La	91
	Rainy	Range test	Ba, Ce, Co, Fe, K, La, Mn	
		LDA	Ba, Ce, Co, Fe, K, La	82

subjective, given its total dependence on the assumptions made by the modeler about potential sources of uncertainty (Beven, 2009). Our approach presents a rather conservative estimate of model uncertainty, basically representing the errors involved in parameter estimation. This is because we could not describe all the sources of error in the model structure. Moreover, we wanted to constrain model realizations based on choices of factor values that modelers are expected to make. Hence, we did not want to give the models full freedom: if all parameters and variables are allowed to vary beyond a range of physical meaning, models are capable of reproducing almost any answer – usually for the wrong reasons (see Batista et al., 2019a).

2.5.1. Spatial representation of model uncertainty

In order to represent the spatial uncertainty of the final SEDD model predictions, we first filtered the behavioral model simulations according to the criterion previously described. Next, we calculated the 2.5%, 50%, and 97.5% quantiles for each grid cell SSY_i estimates. Absolute error grids were then calculated by subtracting the 97.5% grid by the 2.5% grid. Relative errors were determined as:

$$RE_i\ (\%) = \left(\frac{AE_i}{M_i}\right)*100 \quad (5)$$

where: AE_i is the absolute error for a grid cell i, and M_i is the simulation median for grid cell i.

The filtered behavioral model realizations were also used to calculate total sediment yields from the sub-catchments described in Table 1. These calculations were used to estimate the relative contribution of the sub-catchments to the aggregated sediment yields at each sink sampling location (i.e. Nodes 1, 2, and 3). Relative contributions were calculated by dividing individual sub-catchment sediment yields by the sum of all loads from contributing sub-catchments. The SEDD-estimated relative contributions were then evaluated against fingerprinting source apportionments. The same approach was employed for creating RUSLE error maps, except in this case all model simulations, behavioral or not, were considered when calculating grid-cell quantiles.

3. Results

3.1. Discharge curve

The error propagation method used to represent the uncertainty in the sediment rating curve resulted in a broad estimate of average annual specific sediment yields, with a 95% prediction interval of 0.47–11.95 ton ha^{-1} yr^{-1} (mean = 3.45 ton ha^{-1} yr^{-1}; median = 2.52 ton ha^{-1} yr^{-1}) (Fig. 3 a). As expected, annual estimates of sediment loads were more uncertain for the years with greater discharge and sediment transport (Fig. 3 c). Monthly calculations revealed that over 85% of the annual sediment load is transported from November to March. The monthly relative contributions to annual sediment yield showed less uncertainty than annual and average annual estimates (Fig. 3 b).

3.2. Sediment fingerprinting

3.2.1. Element selection

Our exploratory analysis demonstrated that Cu and Zn displayed spurious concentration patterns, as a large proportion of sample measurements (~30%) were below detection limit. These elements were therefore omitted from further scrutiny. Of the remaining 19 elements, 16 (84%), 17 (87%), and nine (47%) plotted within the source mixing polygons for Nodes 1, 2, and 3, respectively, for the dry season (Table 4). For the rainy season, 18 (95%) elements passed the range test for Nodes 1 and 2, whereas only seven (37%) elements were within source range for Node 3 sediments.

For Node 1, the forward step-wise LDA selected 12 elements for the dry season sediments, whereas 11 elements were selected for the rainy season (Table 4). The LDA for both seasons showed a reclassification accuracy of 100%. For Node 2, the discriminant analysis selected 10 elements for the dry season and 11 for the rainy season. Again, all samples were correctly reclassified during the LDA cross-validation. As fewer elements passed the range test for Node 3, only six elements were selected by the LDA for both seasons. Reclassification accuracy was lower in this case, with 91% and 82% for the dry and rainy seasons, respectively. The largest errors associated to the LDA reclassification for Node 3 source samples can be visualized in the bi-plots displayed in Fig. 4.

3.2.2. Un-mixing model results

Un-mixing model solutions for Node 1 were highly uncertain for both seasons, as demonstrated by the broad density curves displayed in Fig. 5. According to model estimates, sources CRD and ELV seem to dominate sediment contributions in relation to MRT and STA, at least considering the median and interquartile (IQR) values of the simulated source apportionments (Table 5).

Results for Node 2 were less uncertain and revealed a greater contrast between seasonal sediment transport dynamics. During the dry season, the un-mixing model indicated that a significant portion of sediments reaching Node 2 are derived from PXE (median = 50%, IQR = 32–64%). However, such contributions decrease during the rainy season, for which the models suggest a large apportion of sediments from Node 1 (median = 60%, IQR = 44–74%). Modeled source contributions from MPQ and T1 were relatively low for both seasons (Table 5).

Model solutions for Node 3 displayed a similar pattern to Node 2 regarding the seasonal variation of source contributions. During the dry season, a greater proportion of sediments were estimated to derive from the sources proximally located to the catchment outlet, particularly TAB (median = 33%, IQR = 15–50%). However, rainy season source apportionments indicate that most of the sediments reaching the Funil reservoir are originated on the upstream areas of the catchment, which are represented by Node 2 (median = 61%, IQR = 34–80%). This illustrates how even in the relative short time-period represented by our study, sediments from the upper- and mid-catchment area are transported throughout the river network. Given that most of the Mortes

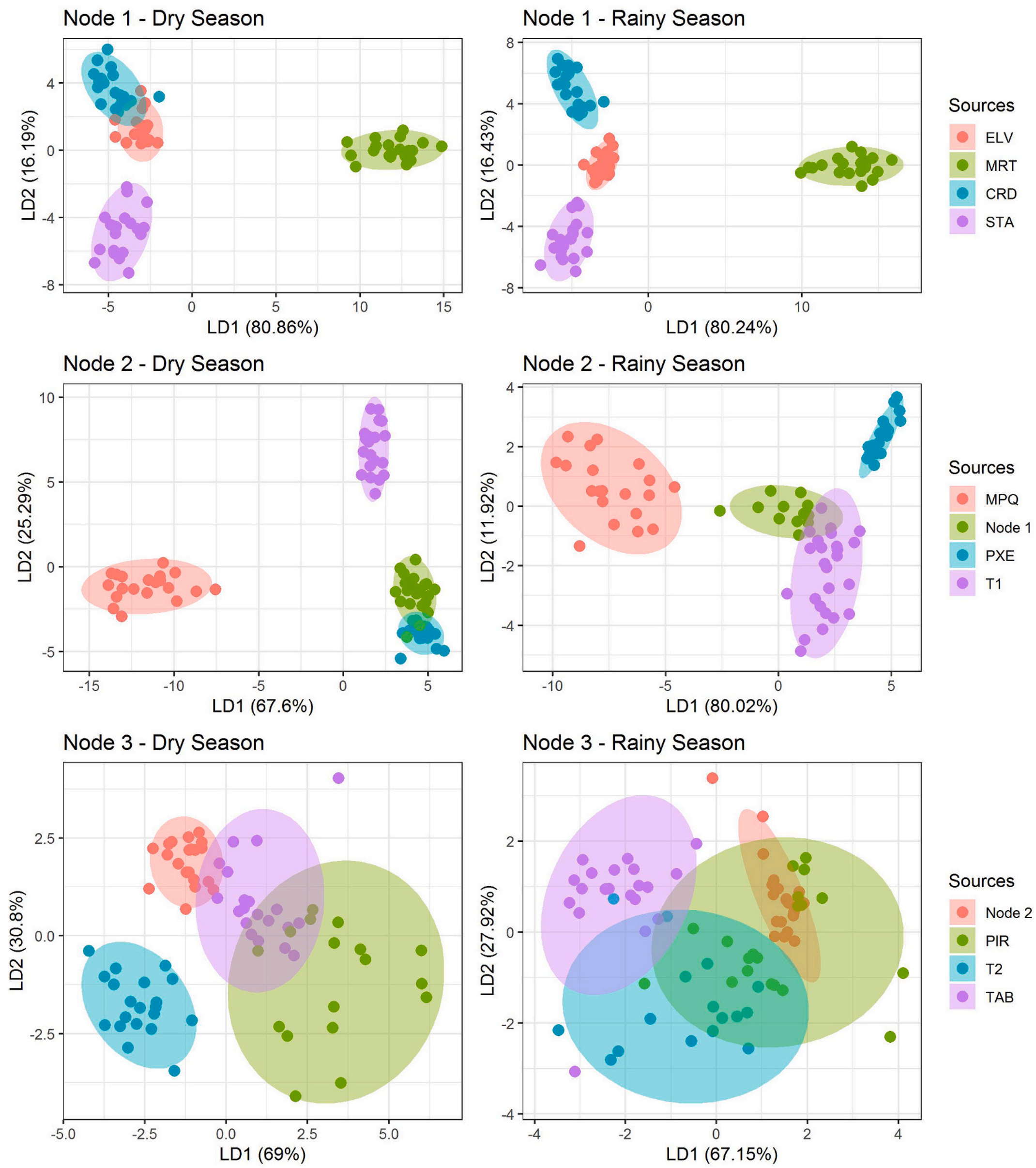

Fig. 4. LDA bi-plots of source reclassification based on selected element concentrations. Ellipses represent 90% confidence intervals. Source locations, names, and abbreviations are defined in Fig. 1.

River sediment load is transported during the rainy season, it is plausible to assume that upstream sediments are important contributors to reservoir sedimentation.

3.3. RUSLE uncertainty

The results of the forward error analysis revealed that RUSLE estimates were highly uncertain in spite of the moderately conservative assumptions made regarding sources of model error. The median of grid cell absolute errors was of 29 ton ha^{-1} yr^{-1}, which translated to a median relative error of 588%. As expected, the highest absolute errors in the RUSLE estimates were associated to the areas with higher erosion rate predictions (Fig. 6 b, c). Contrarily, relative errors were higher on the areas with lower soil loss estimates. This is possibly a result of small variations on sampled parameter values leading to a large relative fluctuation on the low erosion predictions (Fig. 6 a). Considering the median of the simulations as a point-based estimate of erosion rates, the influence of soil erodibility on soil loss predictions was evident in Fig. 6c. Upper- and mid-catchment areas, where Dystrustepts are widespread, had overall higher erosion rates, according to the model simulations. Moreover, modeled erosion hot-spots are visibly associated to areas with high flow accumulation and more intensive land uses (e.g. cropland, eucalypt).

The sensitivity analysis demonstrated that the C factor was the largest source of uncertainty in the model predictions. The proportion of model variance explained by the C factor had a median value of 45% (IQR = 30–56%). The LS (median = 21%; IQR = 17–27%) and K factors (median = 15%; IQR = 10–20%) also contributed significantly to the propagated model errors. The R factor had a small influence on overall model uncertainty (median = 3%, IQR = 2–5%).

3.4. SEDD results

From the 1000 SEDD model realizations generated by the Monte Carlo simulation, 234 were behavioral. That is, 234 model realizations provided estimates of outlet-based SSY within the 95% prediction interval of the sediment rating curve (0.47–11.95 ton ha^{-1} yr^{-1}). Most of the non-behavioral model response surface was associated to an

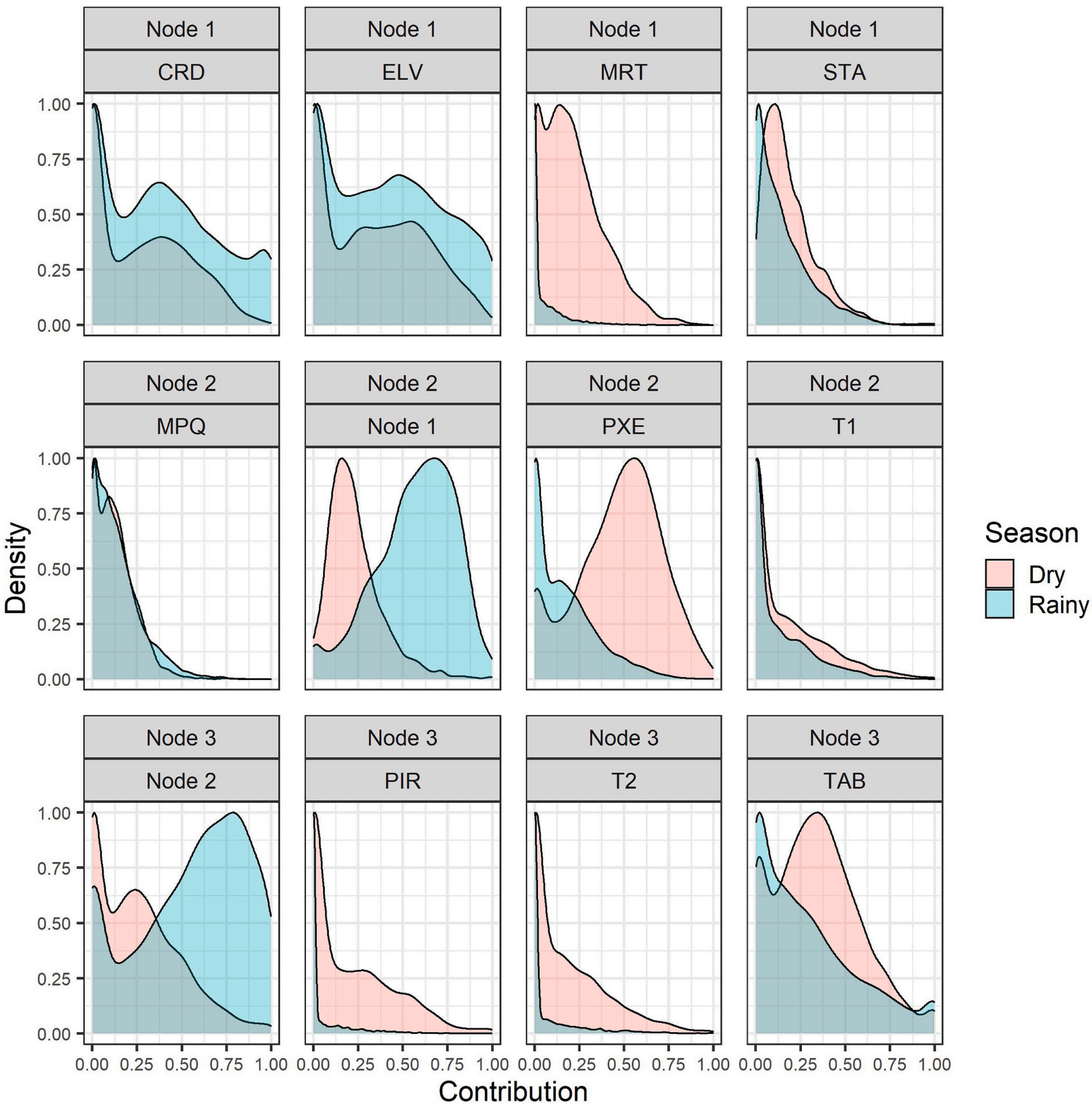

Fig. 5. Probability density functions of estimated relative source contributions. Colors identify the season of the results.

overestimation of the curve-calculated sediment yields (Fig. 7 a).

By analyzing the dotty plots of sampled parameter values, it was clear that the empirical parameter β had a preponderant influence on the model results (Fig. 7 c). Behavioral model realizations are concentrated within a relatively narrow range of β values, whereas acceptable system representations are spread throughout the sampled values of stream definition thresholds. The fluctuation of mean catchment SDR_i values in the catchment led to a linear increment of estimated SSY (Fig. 7 b), indicating little influence of RUSLE simulation results in the outlet-aggregated SEDD model predictions. Behavioral model realizations had mean SDR_i values between 5 and 50%, which highlights the uncertainty in the model predictions.

Considering the median of the behavioral model realizations, grid-cell SSY_i estimates had a median value of 0.06 ton ha^{-1} yr^{-1}, whereas the median of analogous absolute error values was 6.64 ton ha^{-1} yr^{-1}. Although outlet-lumped model results seem to be little influenced by the uncertainty in the RUSLE or in the stream definition threshold, the errors derived from such input variables/parameters are explicit when the uncertainty of spatially distributed SSY estimates are presented in Fig. 8 a. Areas with large absolute errors in the SSY map clearly match the RUSLE errors displayed in Fig. 7 b. Moreover, the influence of stream definition threshold uncertainty is visible in the surroundings of lower order streams.

3.4.1. *Evaluation of SEDD results against fingerprinting source apportionments*

Distributions of relative source contributions estimated by the SEDD model overall displayed a similar pattern to the rainy season fingerprinting source apportionments, except for Node 1 (Fig. 9). Opposite to the fingerprinting results, SEDD simulations indicated that MRT was the main source of sediments (IQR = 52.9–53.4%) reaching the main river channel.

Node 2 results revealed an agreement between rainy season fingerprinting and SEDD-estimated relative source contributions, as all SEDD model realizations were bound by the IQR of the fingerprinting apportionments. However, SEDD simulations calculate an even larger contribution of Node 1 sediments (IQR = 72.6–73.0%). Similarly, fingerprinting results for the rainy season for Node 3 showed a similar

Table 5
Results of the un-mixing models source apportionments based on the Monte Carlo simulations.

Node	Source	Season	2.5% quantile	25% quantile	50% quantile	75% quantile	97.5% quantile
1	CRD	Dry	0.00	0.00	0.25	0.47	0.78
		Rainy	0.00	0.08	0.36	0.62	1.00
	ELV	Dry	0.00	0.00	0.31	0.56	0.88
		Rainy	0.00	0.12	0.41	0.66	1.00
	MRT	Dry	0.00	0.08	0.18	0.31	0.61
		Rainy	0.00	0.00	0.00	0.07	0.33
	STA	Dry	0.00	0.08	0.15	0.26	0.53
		Rainy	0.00	0.02	0.11	0.22	0.55
2	MPQ	Dry	0.00	0.04	0.11	0.18	0.38
		Rainy	0.00	0.04	0.11	0.20	0.47
	Node 1	Dry	0.02	0.13	0.20	0.30	0.62
		Rainy	0.04	0.44	0.60	0.74	0.92
	PXE	Dry	0.00	0.32	0.50	0.64	0.89
		Rainy	0.00	0.00	0.12	0.26	0.60
	T1	Dry	0.00	0.00	0.08	0.28	0.72
		Rainy	0.00	0.00	0.04	0.21	0.58
3	Node 2	Dry	0.00	0.05	0.23	0.41	0.81
		Rainy	0.00	0.34	0.61	0.80	1.00
	PIR	Dry	0.00	0.00	0.13	0.36	0.75
		Rainy	0.00	0.00	0.00	0.07	0.51
	T2	Dry	0.00	0.00	0.12	0.31	0.73
		Rainy	0.00	0.00	0.00	0.09	0.60
	TAB	Dry	0.00	0.17	0.33	0.50	0.88
		Rainy	0.00	0.04	0.22	0.45	1.00

pattern to the SEDD simulations. Both models indicate that Node 2 sediments are the largest contributors to outlet sediment loads, although SEDD results again suggest a greater contribution of upstream sediments (Node 2 IQR = 84.3–85.7%). Moreover, SEDD-estimated TAB contributions (IQR = 3.2–3.4%) were considerably lower than the ones estimated by the sediment fingerprinting un-mixing models.

4. Discussion

4.1. Uncertainty in the forcing data

The model testing framework presented here demonstrated how uncertainty permeates all facets of soil erosion models and the things we call observational data. The error propagation method used to represent the uncertainty in the sediment rating curve resulted in such broad estimates of average annual sediment loads that many different SEDD realizations were able to encompass the forcing data. Similar results have been reported by other soil erosion modelers (Banis et al., 2004; Janes et al., 2018), and a logical conclusion is that we need better data in order to reject non-behavioral model realizations. Importantly, the uncertainty in the average estimates of annual sediment loads highlight how sediment concentration measurements at the Ibituruna gauging station need to be intensified, particularly during high-flow events. By comparing discharge values recorded during the sediment concentration measurements and those observed between 1992 and 2013, it becomes clear that high-flow events may not have been adequately represented by the current sampling regime (Supplementary Material Figs. 2 and 3). Extrapolations of the rating curve for extreme events may therefore result in additional uncertainty in the sediment load estimates. Considering the importance of the Mortes River for hydroelectric power generation, as well as the high sedimentation rates observed at the Funil reservoir, we strongly recommend establishing a thorough water and sediment monitoring program in the catchment.

Nevertheless, even if more accurate and precise sediment load data were available, our approach has demonstrated how very different spatial model representations can produce similar outlet responses. Despite the fact that we only considered behavioral simulations while calculating the uncertainty of grid cell SSY_i estimates, absolute model errors were almost hundred-fold the median of the predictions. This brings to question if the numerical spatial predictions are at all useful. Furthermore, it demonstrates how misleading it can be to neglect model and observational data uncertainty in soil erosion and sediment delivery models.

4.2. Uncertainty in the SEDD model

The fact that the SEDD results were mostly driven by the empirical and somewhat abstract parameter β raises some concerns about the quality of process representation in the model. The common deterministic parameter optimization method for calibrating β should be therefore disputed. If SEDD model simulations are to provide meaningful system representations, alternative methods for deriving β values should be encouraged (e.g. Ferro and Stefano, 2003; Porto and Walling, 2015). Nonetheless, given the sensitivity of the model to parameter β, representing the uncertainty associated to the parameter estimation is paramount.

In spite of the large errors associated to grid cell SSYi estimates, aggregated sub-catchment relative contributions calculated from the SEDD simulations were precise, as shown by the narrow uncertainty bands in Fig. 9. As the sum of the grid-based model realizations should somewhat converge, sub-catchment sediment loads are expected to display smaller variances than the grid cell rates. This demonstrates that, at the very least, spatially aggregated results were consistent, as the model repeatedly identified the same sub-catchments as the main sediment sources. The accuracy of these estimates is difficult to assess, although some insight can be gained by an evaluation against fingerprinting source apportionments.

4.3. Uncertainty in sediment fingerprinting source apportionments

The bootstrapping method for solving the un-mixing models resulted in uncertain sediment fingerprinting estimates of relative source contributions, particularly for Node 1. Bootstrapping methods are known to produce somewhat spurious uncertainty bands for un-mixing model results, as local optimization functions frequently yield numerical solutions where one source provides 0% or 100% of the contributions (Cooper et al., 2014). This is illustrated by the bi-modal density curves in Fig. 4.

Nonetheless, the uncertainty of Node 1 un-mixing model solutions might imply an issue with the data. Moreover, the negligible contributions from MRT (by far the largest sub-catchment in the basin) during the rainy season questions the consistency of the model results as a

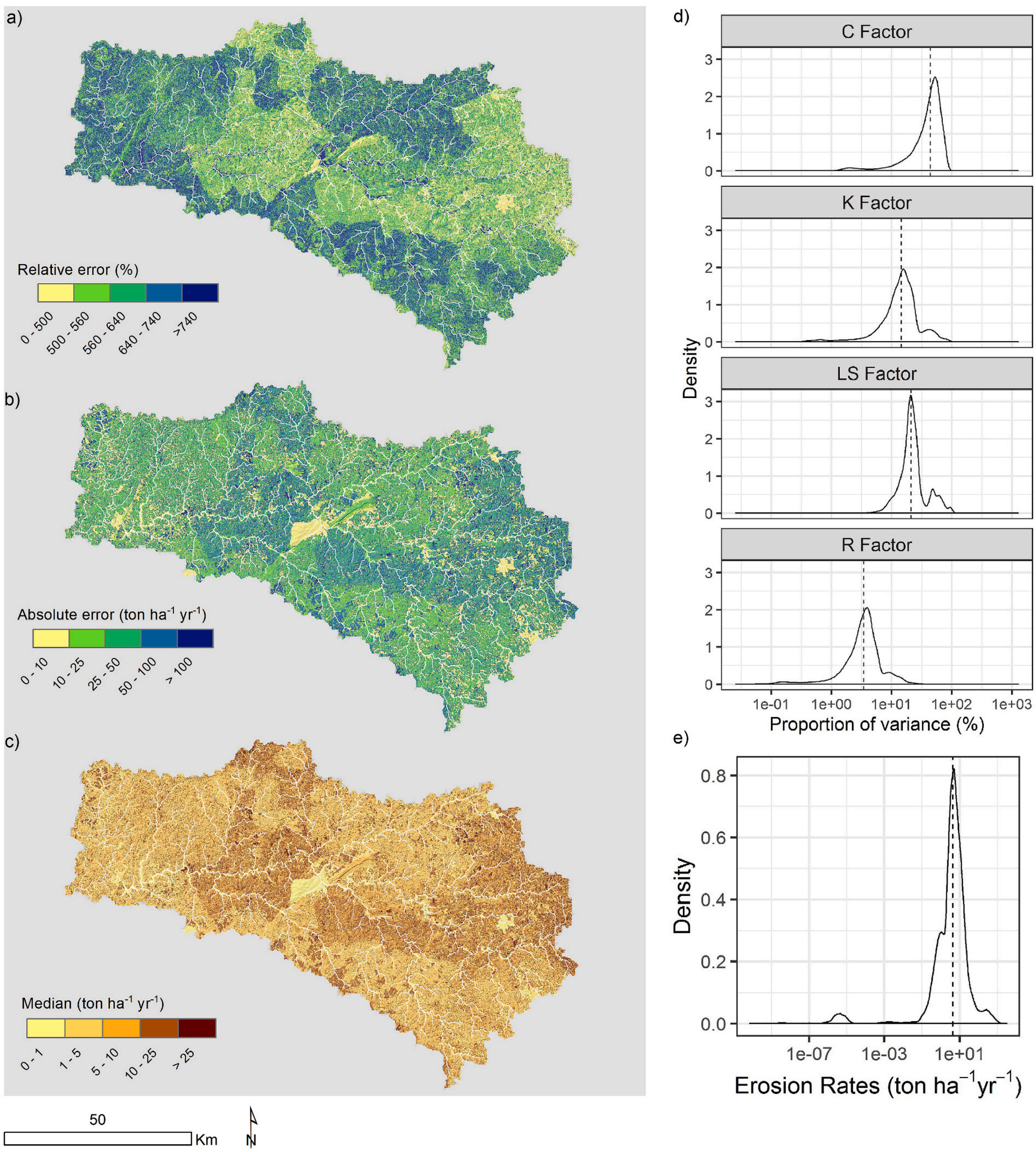

Fig. 6. a) RUSLE relative error map; b) RUSLE absolute error map; c) RUSLE prediction map, based on the median simulation values; d) density curves of the proportion of variance of model error explained by individual RUSLE factors; e) density curve of grid cell erosion rate predictions, based on the median simulation values. Dashed vertical lines represent median values.

narrative. It might be the case that there was an issue of particle size incommensurability between MRT and Node 1 sink sediments. MRT element concentrations were overall higher than in the remaining Node 1 sources and sink samples, which might indicate MRT sediments were composed by smaller-sized particles. An alternative hypothesis is that sediment storage in the MRT sub-catchment is influenced by small hydroelectric plants or channel regulation in the Mortes River before its confluence with the Elvas River. Regardless, fingerprinting and SEDD model outputs showed a contrasting pattern for Node 1, and we have no supporting evidence to corroborate either of the system representations.

On the contrary, the overall correspondence of fingerprinting unmixing model solutions and SEDD simulations of relative source contributions for Nodes 2 and 3, while considering the uncertainty in both system representations, provides some conditional corroboration of the methods. Although the SEDD model simulates long-term sediment transport dynamics and the fingerprinting approach was limited by the temporal scale of our sampling, both modelling exercises designated that most of the sediments reaching Nodes 2 and 3 are originated from farther upstream sources. That is, at least under the reasonable assumption that rainy season fingerprinting results represent the bulk of the sediment transport dynamics in the catchment. For management purposes, the convergence of model results is an important outcome of this research. Different models and sources of data have indicated that the sediments reaching the Funil reservoir by the Mortes River come from the mid- and upper-catchment areas, even during a relatively short temporal scale (i.e. the rainy season covered by the sediment sampling).

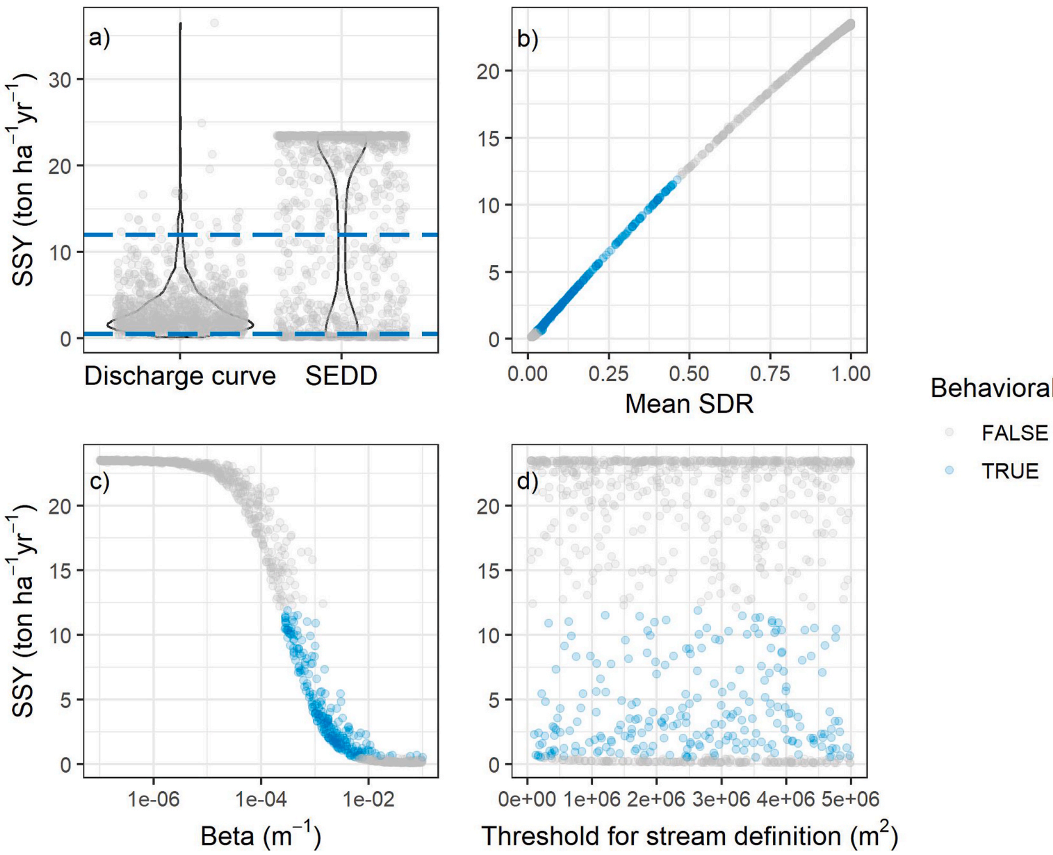

Fig. 7. a) Violin plots of catchment-lumped SSY values estimated by the discharge curve and the SEDD model (dashed lines represent the 95% prediction interval of the discharge curve), b) scatter plot of simulated mean grid cell SDR_i and resulting catchment-lumped SSY values, c) dotty plots of sampled β values, d) dotty plots of sampled threshold for stream definition values.

Hence, reducing reservoir sedimentation rates requires widespread soil conservation efforts throughout the entire catchment, instead of local/proximal interventions.

4.4. Uncertainty in the RUSLE

Another valuable outcome of this research was demonstrating how uncertain common large-scale distributed RUSLE applications are. Although RUSLE is the most widely used soil erosion model in the world (Alewell et al., 2019), studies which have attempted to quantify model error are scarce (e.g. Tetzlaff et al., 2013). Our results indicate that numerical RUSLE predictions of spatially distributed erosion rates lack utility, given the uncertainty in the model outputs (see Fig. 5). Of course, these results are case specific and entirely determined by the assumptions made about potential sources of model error, which we understand, were cautious. That is, the uncertainty in the rainfall erosivity regression equation was not properly assessed, let alone in the equations relating rainfall intensity to kinetic energy (Wilken et al., 2018). Additionally, errors in the soil and land use map classifications were not entirely represented, nor were the potential errors in the plot-based experiments used to generate RUSLE factors (Nearing, 2000; Parsons, 2019). Hence, similar or larger errors should be expected in comparable spatially distributed RUSLE applications elsewhere, unless otherwise demonstrated. Since we were explicit about our assumptions regarding sources of model error, and fully reported the distribution parameters used in the uncertainty analysis, readers can interpret the outputs accordingly. We expect this should attenuate part of the subjectivity necessarily involved in forward uncertainty assessments. Moreover, as model results are reported as distributions, different levels of confidence can be attributed to the simulations according to the potential consequences one might expect from model mispredictions (Quinton, 1997).

Overall, results from our forward error analysis indicate that RUSLE-modeled spatially distributed erosion rates should be viewed with extreme caution, particularly when actual numerical model outputs are used to project the influence of climate and land use changes on future erosion rates. Due to the difficulties involved in large-scale model parameterization, the costs of plot-based experiments for developing empirical model factors, and the multiplicative structure of the RUSLE (and USLE-family models), we suspect that model applications will remain largely uncertain. This might be particularly true for developing countries such as Brazil, where data scarcity further complicates model parameterization. Under such conditions, model testing should hereon focus on evaluating if the models are at least consistently capable of relatively ranking erosion-prone areas, as in Fischer et al. (2018).

Importantly, the high uncertainty associated with the RUSLE predictions contradicts the argument that USLE-type models are less error prone due to their low input requirements. This is corroborated by Schürz et al. (2019), who demonstrated how model parameterization choices could lead to a variation in the order of two magnitudes in USLE-estimated soil losses. These results indicate that large-scale RUSLE simulations are likely to be no less uncertain than more complex process-based models. As pointed out by Favis-Mortlock et al. (2001), there is little justification in adopting the USLE or its derivatives as standards by which to measure the quality of all other models: this makes the evaluation biased towards the standard, and inhibits the development of 'competing' theories. Hence, we suggest that the modelling community should explore alternative options for simulating soil erosion and sediment connectivity, as different models might be more or less adequate according to the purpose, scale, and conditions of

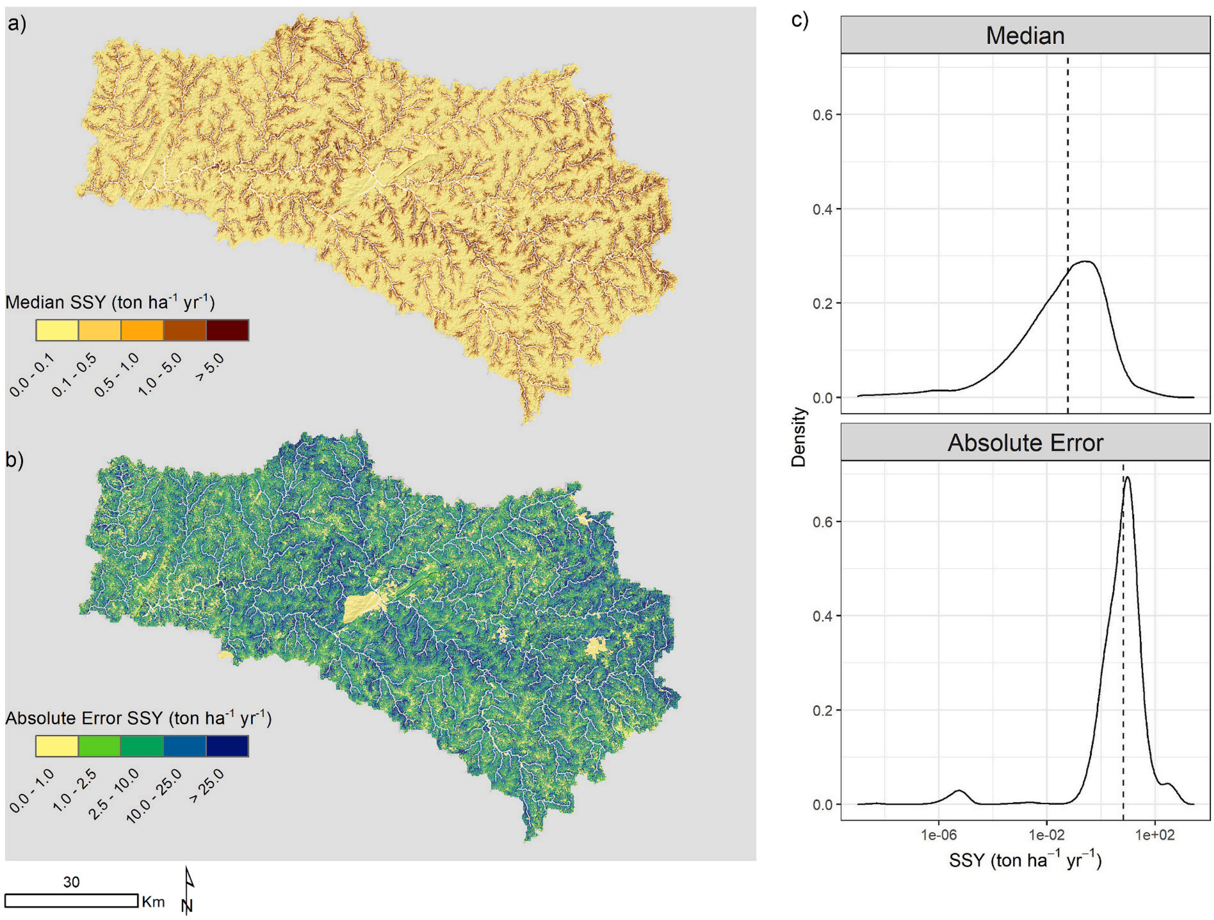

Fig. 8. a) Absolute error of behavioral SEDD simulations, b) median of behavioral SEDD simulations of SSY_i, c) density curves of grid-cell values of absolute model error and median SSY_i simulations. Dashed lines represent the median of the distributions.

the modelling application.

Recent developments with MMF (Eekhout et al., 2018; Peñuela et al., 2018; Smith et al., 2018; Tan et al., 2018), GeoWEPP (Poeppl et al., 2019), and OpenLisem (Baartman et al., 2020; Starkloff et al., 2018) demonstrate how soil erosion models can still be useful tools for understanding processes. Nevertheless, we recommend that any further model evaluation, which is a critical step for developing knowledge and confidence (or doubt) in model predictions, should be firmly established upon an uncertainty-based framework.

4.5. Limitations and future research

An important limitation of the comparison described here between SEDD model outputs and fingerprinting results stems from the temporal divergence of the analyses. While the SEDD model operates on a long-term average annual time-step, our fingerprinting data provided only a snapshot of the sediment dynamics in the catchment. Moreover, the SEDD model does not represent channel erosion and deposition processes, assuming a long-term quasi-equilibrium condition between hillslope sediment yield and the fluvial system. Although our fingerprinting modelling results indicate a strong connectivity between upstream tributaries and the Mortes River outlet, they also demonstrate that transient storage might be an important regulator of the sediment budget in the catchment, as expected. Hence, in order to improve the modelling of the catchment loads, it should be necessary to combine hillslope soil erosion and sediment delivery simulations with models that explicitly account for river sediment dynamics (e.g., Czuba and Foufoula-Georgiou, 2014; Schmitt et al., 2018). Additional modelling and measurement improvements should also investigate the contribution of gullies to catchment sediment loads, as gully erosion was observed in field inspections during the sediment sampling campaigns. Furthermore, future research should focus on elucidating temporal trends in sediment dynamics by use of different fallout radionuclides, such as ^{7}Be and $^{210}Pb_{ex}$ (Evrard et al., 2010; Gellis et al., 2019; Le Gall et al., 2017). This should provide more fit-for-purpose evidence to evaluate soil erosion and sediment delivery models at different time-scales.

5. Conclusions

Soil erosion models and the measurements of system responses we call observational data are necessarily uncertain. The representation of such uncertainty is indispensable. Here we provided a framework for incorporating the uncertainty of sediment rating curves, sediment fingerprinting un-mixing models, and soil erosion/sediment delivery models into the GLUE methodology. More specifically, the framework was applied to the RUSLE-based SEDD model at a large catchment in Southeast Brazil.

Our results have shown how large-scale spatially-distributed RUSLE applications are highly uncertain. This means model applications of such type cannot afford to disregard uncertainty analysis, and that modeled erosion rates should be interpreted with upmost caution. SEDD simulations of catchment sediment yields were also highly uncertain, mostly due to the errors in the rating curve forcing data and the sensitivity of the model to the empirical parameter β. Spatially distributed simulations of area specific sediment yields were even more uncertain, which meant the grid-based numerical model outputs were of little utility. However, when the SEDD model outputs were lumped into sub-catchment relative

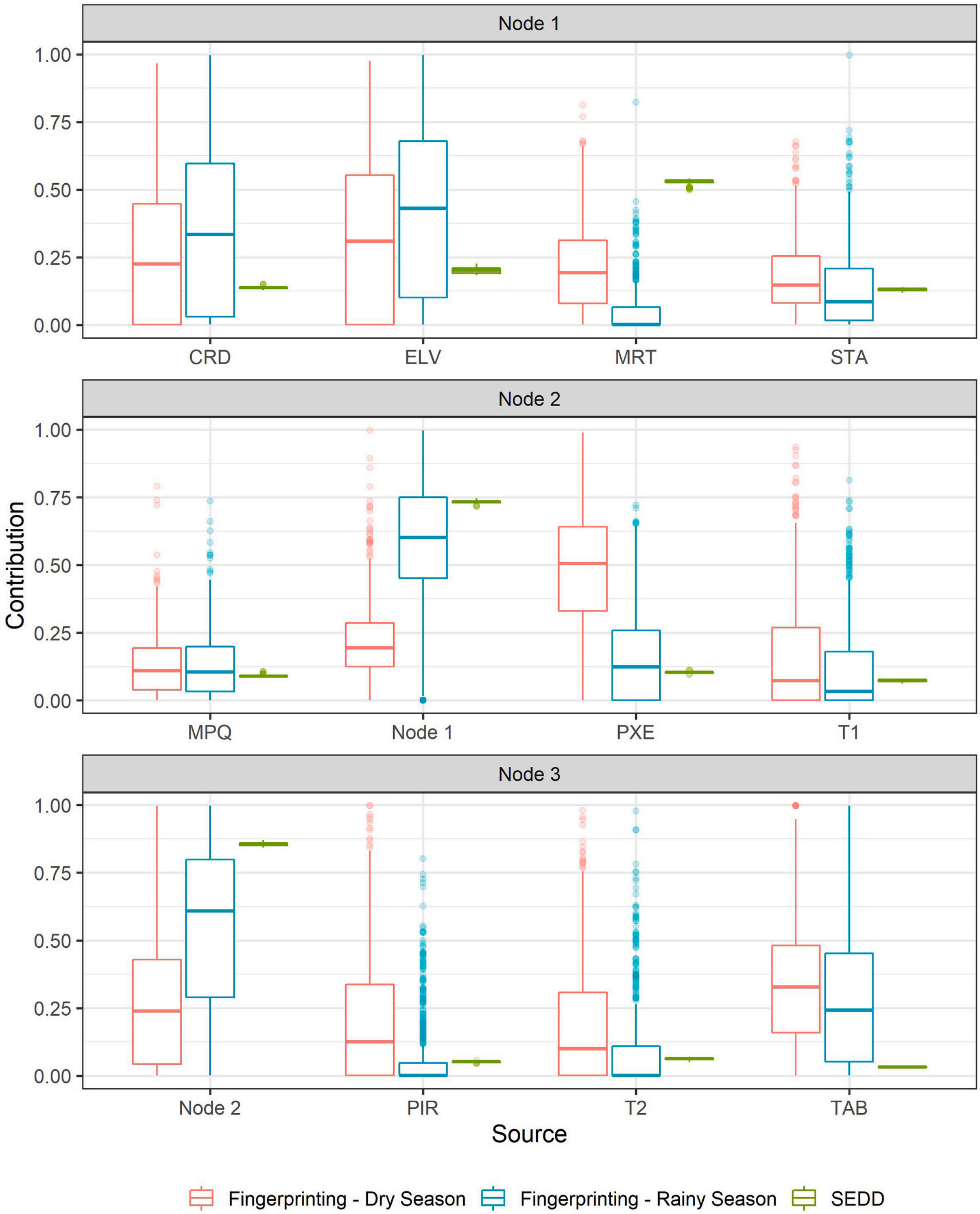

Fig. 9. Relative source contributions estimated by SEDD and fingerprinting un-mixing models.

contributions, results were at least consistent.

The comparison between SEDD model outputs the fingerprinting source apportionments presented here was facilitated by the hierarchical tributary sampling design. Moreover, the uncertainty-based framework enabled us to compare distributions of model realizations of relative source contributions. The comparison revealed an overall similarity of fingerprinting and SEDD-modeled distributions of source apportionments, although large discrepancies were found in part of the catchment.

Ultimately, we found that under the testing conditions, the SEDD model might be useful for identifying the sub-catchments that contribute to most of the sediment load in the Mortes River basin. Conversely, the uncertainty in the simulations questions the model's usefulness for calculating actual erosion and sediment delivery rates. From a falsificationist perspective, the model could not be rejected, as multiple model realizations produced acceptable system representations. However, this was largely facilitated by the uncertainty in the forcing data. One of the most important conclusions from this research is that we need better data in order to reject models (or model realizations) and therefore to improve our understanding of soil erosion and sediment transport in large river catchments. This will require multiple sources of data and honest representations of the uncertainty in models and observations of system responses.

Declaration of competing interest

The authors declare that they have no known competing financial interests or personal relationships that could have appeared to influence the work reported in this paper.

Acknowledgements

This study was funded in part by the Coordination of Improvement of Higher Level Education Personnel – CAPES (process number 88881.190317/2018–01), the National Counsel of Technological and Scientific Development – CNPq (process numbers 306511-2017-7 and 202938/2018–2), and the Minas Gerais State Research Foundation – FAPEMIG (process numbers CAG-APQ-01053-15 and APQ-00802-18). Comments from anonymous reviewers helped to improve the quality of this paper. They are highly appreciated. We are also thankful to Claudia Mignani for helping with our figures and to Tom de Lima for his assistance during field-work.

Appendix A. Supplementary data

Supplementary data to this article can be found online at https://doi.org/10.1016/j.envsoft.2021.104961.

References

Alewell, C., Birkholz, A., Meusburger, K., Schindler Wildhaber, Y., Mabit, L., 2016. Quantitative sediment source attribution with compound-specific isotope analysis in a C3 plant-dominated catchment (central Switzerland). Biogeosciences 13, 1587–1596. https://doi.org/10.5194/bg-13-1587-2016.

Alewell, C., Borelli, P., Meusburger, K., Panagos, P., 2019. Using the USLE: chances, challenges and limitations of soil erosion modelling. Int. Soil Water Conserv. Res. https://doi.org/10.1016/j.iswcr.2019.05.004.

Alvares, C.A., Stape, J.L., Sentelhas, P.C., de Moraes Gonçalves, J.L., Sparovek, G., 2013. Köppen's climate classification map for Brazil. Meteorol. Z. 22, 711–728. https://doi.org/10.1127/0941-2948/2013/0507.

Aquino, R.F., Silva, M.L.N., Freitas, D.A.F., Curi, N., Mello, C.R., Avanzi, J.C., 2014. Erosividade das chuvas e tempo de recorrência para Lavras , Minas Gerais. Ceres 61, 9–16.

Baartman, J.E.M., Nunes, J.P., Masselink, R., Darboux, F., Bielders, C., Degre, A., Cantreul, V., Cerdan, O., Grangeon, T., Fiener, P., Wilken, F., Schindewolf, M., Wainwright, J., 2020. Journal Pre-proof what do models tell us about water and sediment connectivity? Geomorphology 367, 107300. https://doi.org/10.1016/j.geomorph.2020.107300.

Banis, Y.N., Bathurst, J.C., Walling, D.E., 2004. Use of caesium-137 data to evaluate SHETRAN simulated long-term erosion patterns in arable lands. Hydrol. Process. 18, 1795–1809. https://doi.org/10.1002/hyp.1447.

Batista, P.V.G., Davies, J., Silva, M.L.N., Quinton, J.N., 2019a. On the evaluation of soil erosion models : are we doing enough ? Earth Sci. Rev. 197, 102898. https://doi.org/10.1016/j.earscirev.2019.102898.

Batista, P.V.G., Laceby, J.P., Silva, M.L.N., Tassinari, D., Bispo, D.F.A., Curi, N., Davies, J., Quinton, J.N., 2019b. Using pedological knowledge to improve sediment source apportionment in tropical environments. J. Soils Sediments 19, 3274–3289.

Batista, P.V.G., Silva, M.L.N., Silva, B.P.C., Curi, N., Bueno, I.T., Acérbi Júnior, F.W., Davies, J., Quinton, J.N., 2017. Modelling spatially distributed soil losses and sediment yield in the upper Grande River Basin - Brazil. Catena 157, 139–150. https://doi.org/10.1016/j.catena.2017.05.025.

Beven, K.J., 2019. How to make advances in hydrological modelling 1–14. https://doi.org/10.2166/nh.2019.134.

Beven, K.J., 2018. On hypothesis testing in hydrology: why falsification of models is still a really good idea. WIREs Water 5, e1278. https://doi.org/10.1002/wat2.1278.

Beven, K.J., 2009. Environmental Modelling: an Uncertain Future, Environmental Modelling : an Uncertain Future ? Routledge, Oxon.

Beven, K.J., 2006. A manifesto for the equifinality thesis. J. Hydrol. 320, 18–36. https://doi.org/10.1016/j.jhydrol.2005.07.007.

Beven, K.J., Binley, A., 1992. The future of distributed models: model calibration and uncertainty prediction. Hydrol. Process. 6, 279–298. https://doi.org/10.1002/hyp.3360060305.

Biesemans, J., Meirvenne, M. Van, Gabriels, D., 2000. Extending the RUSLE with the Monte Carlo error propagation technique to predict longlterm. J. Soil Water Conserv. 55, 35–42.

Bivant, R., Keitt, T., Rowlingson, B., Pebesma, E., Sumner, M., Hijmans, R., Rouault, E., Warmerdam, F., Ooms, J., Rundel, C., 2019. Rgdal: Bindings for the 'Geospatial'Data Abstraction Library. R Package Version 1, pp. 4–8.

Blake, W.H., Boeckx, P., Stock, B.C., Smith, H.G., Bodé, S., Upadhayay, H.R., Gaspar, L., Goddard, R., Lennard, A.T., Lizaga, I., Lobb, D.A., Owens, P.N., Petticrew, E.L., Kuzyk, Z.Z.A., Gari, B.D., Munishi, L., Mtei, K., Nebiyu, A., Mabit, L., 2018. A deconvolutional Bayesian mixing model approach for river basin sediment source apportionment 1–12. https://doi.org/10.1038/s41598-018-30905-9.

Borrelli, P., Meusburger, K., Ballabio, C., Panagos, P., Alewell, C., 2018. Object-oriented soil erosion modelling: a possible paradigm shift from potential to actual risk assessments in agricultural environments. Land Degrad. Dev. 29, 1270–1281. https://doi.org/10.1002/ldr.2898.

Boudreault, M., Koiter, A.J., Lobb, D.A., Liu, K., Benoy, G., Owens, P.N., Li, S., 2019. Comparison of sampling designs for sediment source fingerprinting in an agricultural watershed in Atlantic Canada. J. Soils Sediments. https://doi.org/10.1007/s11368-019-02306-6.

Calway, R., Weston, S., 2017. Foreach: Provides Foreach Looping Construct for R. R Package, version 1.4.4.

Collins, A.L., Walling, D.E., Leeks, G.J.L., 1997. Source type ascription for fluvial suspended sediment based on a quantitative composite fingerprinting technique. Catena 29, 1–27.

Collins, A.L., Zhang, Y.S., Hickinbotham, R., Bailey, G., Darlington, S., Grenfell, S.E., Evans, R., Blackwell, M., 2013. Contemporary fine-grained bed sediment sources across the river wensum demonstration test catchment, UK. Hydrol. Process. 27, 857–884. https://doi.org/10.1002/hyp.9654.

Conrad, O., Bechtel, B., Bock, M., Dietrich, H., Fischer, E., Gerlitz, L., Wehberg, J., Wichmann, V., Böhner, J., 2015. System for automated geoscientific analyses (SAGA) v . 2 . 1 . 4 1991–2007. https://doi.org/10.5194/gmd-8-1991-2015.

Cooper, R.J., Krueger, T., 2017. An extended Bayesian sediment fingerprinting mixing model for the full Bayes treatment of geochemical uncertainties. Hydrol. Process. 31, 1900–1912. https://doi.org/10.1002/hyp.11154.

Cooper, R.J., Krueger, T., Hiscock, K.M., Rawlins, B.G., 2014. Sensitivity of fluvial sediment source apportionment to mixing model assumptions: a Bayesian model comparison. Water Resour. Res. 50, 9031–9047. https://doi.org/10.1002/2014WR016194 (Received).

Czuba, J.A., Foufoula-Georgiou, E., 2014. A network-based framework for identifying potential synchronizations and amplifications of sediment delivery in river basins. Water Resour. Res. 50, 3826–3851. https://doi.org/10.1002/2013WR014227.

de Vente, J., Poesen, J., Verstraeten, G., Van Rompaey, A., Govers, G., 2008. Spatially distributed modelling of soil erosion and sediment yield at regional scales in Spain. Global Planet. Change 60, 393–415. https://doi.org/10.1016/j.gloplacha.2007.05.002.

Didoné, E.J., Paolo, J., Minella, G., Merten, G.H., 2015. Quantifying soil erosion and sediment yield in a catchment in southern Brazil and implications for land conservation Quantifying soil erosion and sediment yield in a catchment in southern Brazil and implications for land conservation. J. Soils Sediments. https://doi.org/10.1007/s11368-015-1160-0.

Eekhout, J.P.C., Terink, W., de Vente, J., 2018. Assessing the large-scale impacts of environmental change using a coupled hydrology and soil erosion model. Earth Surf. Dyn. Discuss. 1–27. https://doi.org/10.5194/esurf-2018-25.

Evans, R., Brazier, R., 2005. Evaluation of modelled spatially distributed predictions of soil erosion by water versus field-based assessments. Environ. Sci. Pol. 8, 493–501. https://doi.org/10.1016/j.envsci.2005.04.009.

Evrard, O., Némery, J., Gratiot, N., Duvert, C., Ayrault, S., Lefèvre, I., Poulenard, J., Prat, C., Bonté, P., Esteves, M., 2010. Sediment dynamics during the rainy season in tropical highland catchments of central Mexico using fallout radionuclides. Geomorphology 124 (1–2), 42–54. https://doi.org/10.1016/j.geomorph.2010.08.007.

Evrard, O., Poulenard, J., Némery, J., Ayrault, S., Gratiot, N., Duvert, C., Prat, C., Lefèvre, I., Bonté, P., Esteves, M., 2013. Tracing sediment sources in a tropical highland catchment of central Mexico by using conventional and alternative fingerprinting methods. Hydrol. Process. 27, 911–922. https://doi.org/10.1002/hyp.9421.

Favis-Mortlock, D., Boardman, J., MacMillan, V., 2001. Landscape Erosion and Evolution Modeling. Springer US, Boston, MA. https://doi.org/10.1007/978-1-4615-0575-4.

FEAM - Fundação Estadual Do Meio Ambiente, 2010. Mapa de solos de Minas Gerais: legenda expandida. FEAM/UFV/CETEC/UFLA, Belo Horizonte. Brazil.

Fernandez, C., Wu, J.Q., Mccool, D.K., Stockle, C.O., 2003. Estimating water erosion and sediment yield with GIs , RUSLE , and SEDD. J. Soil Water Conserv. 58, 128–136.

Ferro, V., Minacapilli, M., 1995. Sediment delivery processes at basin scale. Hydrol. Sci. J. 40, 703–717. https://doi.org/10.1080/02626669509491460.

Ferro, V., Porto, P., 2000. Sediment delivery distributed (SEDD) model. J. Hydrol. Eng. 411–422.

Ferro, V., Stefano, C.D.I., 2003. Calibrating the SEDD Model for Sicilian Ungauged Basins.

Fick, S.E., 2017. WorldClim 2 : New 1-km Spatial Resolution Climate Surfaces for Global Land Areas 4315, pp. 4302–4315. https://doi.org/10.1002/joc.5086.

Fischer, F.K., Kistler, M., Brandhuber, R., Maier, H., Treisch, M., Auerswald, K., 2018. Validation of official erosion modelling based on high-resolution radar rain data by aerial photo erosion classification. Earth Surf. Process. Landforms 43, 187–194. https://doi.org/10.1002/esp.4216.

Fu, G., Chen, S., McCool, D.K., 2006. Modeling the impacts of no-till practice on soil erosion and sediment yield with RUSLE, SEDD, and ArcView GIS. Soil Tillage Res. 85, 38–49. https://doi.org/10.1016/j.still.2004.11.009.

Gellis, A.C., Fuller, C.C., Van Metre, P., Filstrup, C.T., Tomer, M.D., Cole, K.J., Sabitov, T. Y., 2019. Combining sediment fingerprinting with age-dating sediment using fallout radionuclides for an agricultural stream, Walnut Creek, Iowa, USA. J. Soils Sediments 19 (9), 3374–3396. https://doi.org/10.1007/s11368-018-2168-z.

Gelman, A., Hill, J., 2007. Data Analysis Using Regression and Multilevel/Hierarchical Models. Cambridge Univeristy Press, New York.

Ghalanos, A., Theussl, S., 2015. Rsolnp: General Non-linear Optimization Using Augmented Lagrange Multiplier Method. R Package Version 1.16.

Govers, G., 2011. Misapplications and misconceptions of erosion models. In: Morgan, R. P.C., Nearing, M.A. (Eds.), Handbook of Erosion Modelling. Blackwell Publishing Ltd., Chichester, pp. 117–134.

Hijmans, Van Etten, 2012. Raster: geographic analysis and modelling with raster data. R package version 2, 5–8.

Jain, P., Ramsankaran, R.A.A.J., 2018. GIS-based modelling of soil erosion processes using the modified-MMF (MMMF) model in a large watershed having vast agro-climatological differences. Earth Surf. Process. Landforms 43, 2064–2076. https://doi.org/10.1002/esp.4372.

Janes, V., Holman, I., Birkinshaw, S., O'Donnell, G., Kilsby, C., 2018. Improving bank erosion modelling at catchment scale by incorporating temporal and spatial variability. Earth Surf. Process. Landforms 43, 124–133. https://doi.org/10.1002/esp.4149.

Jetten, V., Govers, G., Hessel, R., 2003. Erosion models: quality of spatial predictions. Hydrol. Process. 17, 887–900. https://doi.org/10.1002/hyp.1168.

Klages, M.G., Hsieh, Y.P., 1975. Suspended solids carried by the Gallatin River of Southwestern Montana: II. Using mineralogy for inferring sources. J. Environ. Qual. 4, 68–73.

Koiter, A.J., Lobb, D.A., Owens, P.N., Petticrew, E.L., Tiessen, K.H.D., Li, S., 2013. Investigating the role of connectivity and scale in assessing the sources of sediment in an agricultural watershed in the Canadian prairies using sediment source fingerprinting. J. Soils Sediments 13, 1676–1691. https://doi.org/10.1007/s11368-013-0762-7.

Krasa, J., Dostal, T., Jachymova, B., Bauer, M., Devaty, J., 2019. Soil erosion as a source of sediment and phosphorus in rivers and reservoirs – watershed analyses using WaTEM/SEDEM. Environ. Res. 171, 470–483. https://doi.org/10.1016/j.envres.2019.01.044.

Laceby, J.P., Evrard, O., Smith, H.G., Blake, W.H., Olley, J.M., Minella, J.P.G., Owens, P. N., 2017. The challenges and opportunities of addressing particle size effects in sediment source fingerprinting : a review. Earth Sci. Rev. 169, 85–103. https://doi.org/10.1016/j.earscirev.2017.04.009.

Laceby, J.P., McMahon, J., Evrard, O., Olley, J., 2015. A comparison of geological and statistical approaches to element selection for sediment fingerprinting. J. Soils Sediments 15, 2117–2131. https://doi.org/10.1007/s11368-015-1111-9.

Laceby, J.P., Olley, J., 2015. An examination of geochemical modelling approaches to tracing sediment sources incorporating. In: An Examination of Geochemical Modelling Approaches to Tracing Sediment Sources Incorporating Distribution Mixing and. https://doi.org/10.1002/hyp.10287.

Lacoste, M., Michot, D., Viaud, V., Evrard, O., Walter, C., 2014. Combining137Cs measurements and a spatially distributed erosion model to assess soil redistribution in a hedgerow landscape in northwestern France (1960-2010). Catena 119, 78–89. https://doi.org/10.1016/j.catena.2014.03.004.

Langfelder, P., Horvath, S., 2019. WGCNA: Weighted Correlation Network Analysis. R package version 1.69.

Le Gall, M., Evrard, O., Foucher, A., Laceby, J.P., Salvador-Blanes, S., Manière, L., Lefèvre, I., Cerdan, O., Ayrault, S., 2017. Investigating the temporal dynamics of suspended sediment during flood events with 7 Be and 210 Pb xs measurements in a drained lowland catchment. Sci. Rep. 7 (February), 1–10. https://doi.org/10.1038/srep42099.

Lin, C., Wu, Z., Ma, R., Su, Z., 2016. Detection of sensitive soil properties related to non-point phosphorus pollution by integrated models of SEDD and PLOAD. Ecol. Indicat. 60, 483–494. https://doi.org/10.1016/j.ecolind.2015.07.023.

Mersmann, O., Trautmann, H., Steuer, D., Bornkamp, B. Truncnorm: Density, Probability, Quantile and Random Number Generation Functions for the Truncated Normal Distribution. R Package Version 1.0-8.

Morgan, R.P.C., 2001. A simple approach to soil loss prediction: a revised Morgan-Morgan-Finney model. Catena 44, 305–322. https://doi.org/10.1016/S0341-8162(00)00171-5.

Morgan, R.P.C., Morgan, D.D.V., Finney, H.J., 1984. A predictive model for the assessment of soil erosion risk. J. Agric. Eng. Res. 30, 245–253. https://doi.org/10.1016/S0021-8634(84)80025-6.

Nearing, M.A., 2000. Evaluating soil erosion models using measured plot data: accounting for variability in the data. Earth Surf. Process. Landforms 25, 1035–1043. https://doi.org/10.1002/1096-9837(200008)25:9<1035::AID-ESP121>3.0.CO;2-B.

Ooi, H., , Microsoft Corporation, Weston, S., Tenenbaum, D., 2019. doParallel: Foreach Parallel Adaptor for the 'parallel'Package. R package version 1.0.15.

Oreskes, N., Belitz, K., 2001. Philosophical issues in model assessment. In: Anderson, M. G., Bates, P.D. (Eds.), Model Validation: Perspectives in Hydrological Science. John Wiley & Sons, pp. 23–41.

Panagos, P., Borrelli, P., Meusburger, K., 2015. A new European slope length and steepness factor (LS-Factor) for modeling soil erosion by water. Geosciences 5, 117–126. https://doi.org/10.3390/geosciences5020117.

Parsons, A.J., 2019. How reliable are our methods for estimating soil erosion by water? Sci. Total Environ. 676, 215–221. https://doi.org/10.1016/j.scitotenv.2019.04.307.

Parsons, A.J., Wainwright, J., Brazier, R.E., Powell, D.M., 2009. Is sediment delivery a fallacy? Earth Surf. Process. Landforms 34, 155–161. https://doi.org/10.1002/esp.

Peñuela, A., Sellami, H., Smith, H.G., 2018. A model for catchment soil erosion management in. humid agricultural environments 622, 608–622. https://doi.org/10.1002/esp.4271.

Poeppl, R.E., Dilly, L.A., Haselberger, S., Renschler, C.S., Baartman, J.E.M., 2019. Combining soil erosion modeling with connectivity analyses to assess lateral fine sediment input into agricultural streams. Water (Switzerland) 11. https://doi.org/10.3390/w11091793.

Pontes, L.M., 2017. Hydrosedimentological modeling in the Jaguarí river basin. (PhD thesis) Universidade Federal de Lavras.

Porto, P., Walling, D.E., 2015. Use of caesium-137 measurements and long-term records of sediment load to calibrate the sediment delivery component of the SEDD model and explore scale effect: examples from southern Italy. J. Hydrol. Eng. 20, C4014005 https://doi.org/10.1061/(ASCE)HE.1943-5584.0001058.

Quinton, J.N., 1997. Reducing predictive uncertainty in model simulations: a comparison of two methods using the European Soil Erosion Model (EUROSEM). Catena 30, 101–117.

R Development Core Team, 2017. R: A Language and Environment for Statistical Computing.

Rodriguez, E., Morris, C., Belz, J., 2006. An assessment of the SRTM topographic products. Photogramm. Eng. Rem. Sens. 12, 249–260. https://doi.org/10.14358/PERS.72.3.249.

Rustomji, P., Wilkinson, S.N., 2008. Applying bootstrap resampling to quantify uncertainty in fluvial suspended sediment loads estimated using rating curves 44. https://doi.org/10.1029/2007WR006088, 1-12.

Schmidt, S., Tresch, S., Meusburger, K., 2019. MethodsX Modi fi cation of the RUSLE slope length and steepness factor (LS-factor) based on rainfall experiments at steep alpine grasslands. Methods 6, 219–229. https://doi.org/10.1016/j.mex.2019.01.004.

Schmitt, R.J.P., Bizzi, S., Castelletti, A.F., Kondolf, G.M., 2018. Stochastic modeling of sediment connectivity for reconstructing sand fluxes and origins in the unmonitored Se kong, Se san, and sre pok tributaries of the mekong river. J. Geophys. Res. Earth Surf. 123, 2–25. https://doi.org/10.1002/2016JF004105.

Schürz, C., Mehdi, B., Kiesel, J., Schulz, K., Herrnegger, M., 2019. A systematic assessment of uncertainties in large scale soil loss estimation from different representations of USLE input factors – a case study for Kenya and Uganda. Hydrol. Earth Syst. Sci. Discuss. 1–35. https://doi.org/10.5194/hess-2019-602.

Silva, M.L.N., Quinton, J.N., Cândido, B.M., Curi, N., Batista, P.V.G., Cardoso, P., Avalos, F.A., Davies, J., 2019. (R)USLE factors obtained in standard plots: a crital analysis, opportunities and challenges related to the database in Brazil. In: Proceedings of the Global Symposium on Soil Erosion. Italy, Rome.

Smith, H.G., Blake, W.H., 2014. Sediment fingerprinting in agricultural catchments: a critical re-examination of source discrimination and data corrections. Geomorphology 204, 177–191. https://doi.org/10.1016/j.geomorph.2013.08.003.

Smith, H.G., Karam, D.S., Lennard, A.T., 2018a. Evaluating tracer selection for catchment sediment fingerprinting. J. soils. https://doi.org/10.1007/s11368-018-1990-7.

Smith, H.G., Peñuela, A., Sangster, H., Sellami, H., Boyle, J., Chiverrell, R., Schillereff, D., Riley, M., 2018b. Simulating a century of soil erosion for agricultural catchment management. Earth Surf. Process. Landforms 43, 2089–2105. https://doi.org/10.1002/esp.4375.

Starkloff, T., Stolte, J., Hessel, R., Ritsema, C., Jetten, V., 2018. Integrated, spatial distributed modelling of surface runoff and soil erosion during winter and spring. Catena 166, 147–157. https://doi.org/10.1016/j.catena.2018.04.001.

Taguas, E.V., Moral, C., Ayuso, J.L., Pérez, R., Gómez, J.a., 2011. Modeling the spatial distribution of water erosion within a Spanish olive orchard microcatchment using the SEDD model. Geomorphology 133, 47–56. https://doi.org/10.1016/j.geomorph.2011.06.018.

Takken, I., Beuselinck, L., Nachtergaele, J., Govers, G., Poesen, J., Degraer, G., 1999. Spatial evaluation of a physically-based distributed erosion model (LISEM). Catena 37, 431–447. https://doi.org/10.1016/S0341-8162(99)00031-4.

Tanyaş, H., Kolat, Ç., Süzen, M.L., 2015. A new approach to estimate cover-management factor of RUSLE and validation of RUSLE model in the watershed of Kartalkaya Dam. J. Hydrol. 528, 584–598. https://doi.org/10.1016/j.jhydrol.2015.06.048.

Tan, Z., Leung, L.R., Li, H., Tesfa, T., 2018. Modelling sediment yield in land surface and earth system models: model comparison, development, and evaluation. J. Adv. Model. Earth Syst. 10, 2192–2213. https://doi.org/10.1029/2017MS001270.

Tetzlaff, B., Friedrich, K., Vorderbrügge, T., Vereecken, H., Wendland, F., 2013. Distributed modelling of mean annual soil erosion and sediment delivery rates to surface waters. Catena 102, 13–20. https://doi.org/10.1016/j.catena.2011.08.001.

Van Oost, K., Govers, G., Cerdan, O., Thauré, D., Van Rompaey, a., Steegen, a., Nachtergaele, J., Takken, I., Poesen, J., 2005. Spatially distributed data for erosion model calibration and validation: the Ganspoel and Kinderveld datasets. Catena 61, 105–121. https://doi.org/10.1016/j.catena.2005.03.001.

Van Oost, K., Govers, G., Desmet, P.J.J., 2000. Evaluating the effects of changes in landscape structure on soil erosion by water and tillage. Landsc. Ecol. 15, 577–589. https://doi.org/10.1023/A:1008198215674.

Van Rompaey, A.J.J., Govers, G., 2002. Data quality and model complexity for regional scale soil erosion prediction. Int. J. Geogr. Inf. Sci. 16, 663–680. https://doi.org/10.1080/13658810210148561.

Van Rompaey, A.J.J., Verstraeten, G., Van Oost, K., Govers, G., Poesen, J., 2001. Modelling mean annual sediment yield using a distributed approach. Earth Surf. Process. Landforms 26, 1221–1236. https://doi.org/10.1002/esp.275.

Verstraeten, G., Van Oost, K., Van Rompaey, A.J.J., Poesen, J., Govers, G., 2010. Evaluating an integrated approach to catchment management to reduce soil loss and sediment pollution through modelling. Soil Use Manag. 18, 386–394. https://doi.org/10.1111/j.1475-2743.2002.tb00257.x.

Vigiak, O., Bende-michl, U., 2013. Estimating Bootstrap and Bayesian Prediction Intervals for Constituent Load Rating Curves 49, pp. 8565–8578. https://doi.org/10.1002/2013WR013559.

Vigiak, O., Malagó, A., Bouraoui, F., Vanmaercke, M., Poesen, J., 2015. Adapting SWAT hillslope erosion model to predict sediment concentrations and yields in large Basins. Sci. Total Environ. 538, 855–875. https://doi.org/10.1016/j.scitotenv.2015.08.095.

Walling, D.E., He, Q., Whelan, P.A., 2003. Using 137Cs measurements to validate the application of the AGNPS and ANSWERS erosion and sediment yield models in two small Devon catchments. Soil Tillage Res. 69, 27–43. https://doi.org/10.1016/S0167-1987(02)00126-5.

Walling, D.E., Woodward, J.C., 1995. Tracing sources of suspended sediment in river basins: a case study of the River Clum, Devon, UK. Mar. Freshw. Res. 46, 327–336.

Warren, S.D., Mitasova, H., Hohmann, M.G., Landsberger, S., Iskander, F.Y., Ruzycki, T. S., Senseman, G.M., 2005. Validation of a 3-D enhancement of the Universal Soil Loss Equation for prediction of soil erosion and sediment deposition. Catena 64, 281–296. https://doi.org/10.1016/j.catena.2005.08.010.

Wilken, F., Baur, M., Sommer, M., Deumlich, D., Bens, O., Fiener, P., 2018. Uncertainties in rainfall kinetic energy-intensity relations for soil erosion modelling. Catena 171, 234–244. https://doi.org/10.1016/j.catena.2018.07.002.

Wilkinson, S.N., Hancock, G.J., Bartley, R., Hawdon, A.a., Keen, R.J., 2013. Using sediment tracing to assess processes and spatial patterns of erosion in grazed rangelands, Burdekin River basin, Australia. Agric. Ecosyst. Environ. 180, 90–102. https://doi.org/10.1016/j.agee.2012.02.002.

Wilkinson, S.N., Olley, J.M., Furuichi, T., Burton, J., Kinsey-Henderson, A.E., 2015. Sediment source tracing with stratified sampling and weightings based on spatial gradients in soil erosion. J. Soils Sediments 15, 2038–2051. https://doi.org/10.1007/s11368-015-1134-2.

Wilkinson, S.N., Prosser, I.P., Rustomji, P., Read, A.M., 2009. Modelling and testing spatially distributed sediment budgets to relate erosion processes to sediment yields. Environ. Model. Software 24, 489–501. https://doi.org/10.1016/j.envsoft.2008.09.006.

Yu, L., Oldfield, F., 1989. A multivariate mixing model for identifying sediment source from from magnetic measurements. Quat. Res. 32, 168–181.

Zweifel, L., Meusburger, K., Alewell, C., 2019. Spatial-temporal pattern of soil degradation in a Swiss Alpine grassland catchment. Remote Sens. Environ. 235, 111441.